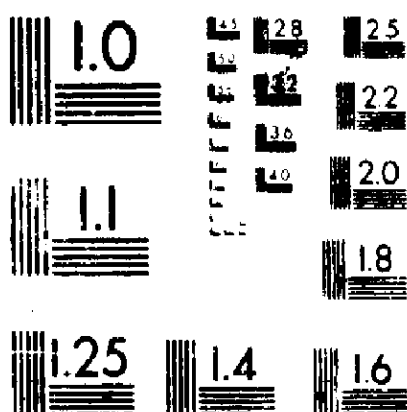MICROCOPY RESOLUTION TEST CHART
NATIONAL BUREAU OF STANDARDS
STANDARD REFERENCE MATERIAL 1010a
(ANSI and ISO TEST CHART No. 2)

NASA Technical Memorandum 89124

SIMULATED MEASUREMENT OF POWER FLOW IN STRUCTURES NEAR TO SIMPLE SOURCES AND SIMPLE BOUNDARIES

MICHAEL C. McGARY

JUNE 1988

SUMMARY

Recent advances in electronics technology along with the advent of low cost multi-channel Fast Fourier analyzers have now made it practical to use higher order central difference formulae to measure power flow in one dimensional and two dimensional structures. The method discussed in this paper uses five point differencing for the spatial derivatives in one dimension and a thirteen point difference pattern for the spatial derivatives in two dimensional plates and shells. It is assumed that the measuring transducers are accelerometers.

An analytical study of the higher order differencing method and the conventional two accelerometer method was performed here as a preliminary to the application of these methods to actual aircraft structures. Some classical problems were analyzed in order to simulate and compare the performance of the two methods under near field measurement conditions. Near field conditions analyzed in this study include examples of power flows near simple sources and simple boundaries. The estimates produced by the two methods were compared to the exact solution in each example. This paper presents the theory and selected results of the study. The results indicate that the bias errors of the two accelerometer method under near field measurement conditions may be much larger than previous studies have suggested.

INTRODUCTION

The successful realization of a diagnostic measurement device for measuring power flow would greatly aid design engineers in their efforts to reduce the aircraft interior noise and vibration of both fixed wing and rotary wing aircraft.

1

For example, accurate power flow measurements would allow designers to determine the critical paths of the vibrational energy transmission through the various structural members, verify computer predictions produced by sophisticated analytical models, and determine the relative level of effectiveness of various treatment methods used in reducing the vibrational power transmission in a structure.

In order for a power flow measurement method to be utilized to its fullest potential on aircraft structures it must meet the following operational requirements:

(1) The method must be accurate when measuring in evanescent or reverberant flow fields.

(2) The method must be applicable to a variety of aircraft structures with different material properties and aspect ratios.

(3) The method must be applicable over a wide range of frequencies.

Nearly all of the research performed in the past fifteen years on experimental measurement methods for measuring power flow in structures has focused on the two accelerometer method.[1] " In order to circumvent the difficulties of keeping track of the multiplicity of terms required to measure power flow, the two accelerometer method utilizes several simplifying assumptions, sometimes called Noiseux's assumptions[1], which are based on the premise that the shear wave component and the bending wave component are equal under "free field" measurement conditions. (A "free field" contains no power sources or boundaries in the vicinity of the transducers.)

As a result of the use of these assumptions, it was known at the outset that the data obtained by Noiseux's method would be inaccurate near power sources or boundaries and that only an estimate of the total power flow with no shear-bending-twist component breakdown would be possible. The method has remained

2

popular, however, since it requires only two transducers for measurements in a one dimensional structure (four transducers for a two dimensional structure) and only a dual channel Fast Fourier analyzer to perform the spectral analysis of the data. Largely due to the simplicity of the measurement system, this method appears to have become widely accepted for measuring power flow in simple beams and plates. The two principal difficulties with the method have been identified by researchers as inaccuracies while measuring under near-field conditions[4,6], and signal-to-noise problems associated with highly reveberant measurement conditions.[4,5]

Recent advances in electronics technology along with the advent of low cost multi-channel Fast Fourier analyzers have now made it possible to use more sophisticated methods to measure power flow in one dimensional and two dimensional structures. Extremely low weight (0.3 gram) miniature piezoelectric accelerometers can now be used in conjuction with a multi-channel Fast Fourier analyzer to perform power flow measurements. The method proposed in this paper (based in part on Pavic's earlier work[2]) performs a direct finite difference approximation of the spatial derivatives by utilizing a 13 accelerometer computational molecule for the two dimensional problem (5 accelerometers for the one dimensional problem). The primary advantage of this method is that its results remain accurate near power sources and boundaries and it provides a shear-bending-twist component breakdown of the total power flow. (With the large number of power sources and the hundreds of structural junctures and boundaries in an aircraft, these improvements are believed to be essential.)

As a first step in applying this new method to aircraft structures, an analytical study of the new method and the older two accelerometer method was performed in order to simulate and compare the performance of the two methods under near field measurement conditions. Measurement conditions analyzed in

3

this study include simulated measurements near line forces, line moments, point forces, point moments, lateral quadrupoles, and near boundaries which possess various combinations of mass, translational stiffness, mass moment of inertia, and rotational stiffness properties. The predicted results of the two methods were compared to the exact solution in each case. This paper outlines the theory utilized in this study and presents the computed results for the simulated near field measurement conditions.

SYMBOLS

a^+	amplitude vector of a right traveling wave at position $x = 0$
a^-	amplitude vector of a left traveling wave at position $x = 0$
$a^+(x)$	amplitude vector of a right traveling wave at position x
$a^-(x)$	amplitude vector of a left traveling wave at position x
B	bending stiffness of the plate given by the expression $Eh^3/[12(1-\mu^2)]$
C_1, C_2	arbitrary amplitude coefficients used in the general solution of the
C_3, C_4	governing equation
C_η	reflection matrix coefficient used to represent the translational stiffness and inertia
C_θ	reflection matrix coefficient used to represent the rotational stiffness and inertia
e	base of the natural logarithms
E	Young's modulus (modulus of elasticity)
f	frequency
$[f]$	propagation matrix for a right traveling wave
$[f]^{-1}$	propagation matrix for a left traveling wave
F_p	amplitude (source strength) of a point force input
$G_{\alpha\alpha}$	auto spectrum of acceleration signal α ($\alpha = 1, 2, 3 \ldots 13$)
$G_{\alpha\beta}$	cross spectrum of acceleration signals α and β ($\alpha, \beta = 1, 2, 3 \ldots 13$)

4

h	plate thickness
$H_0^{(1)}()$	0th order Hankel function of the first kind
$H_0^{(2)}()$	0th order Hankel function of the second kind
$H_1^{(2)}()$	1st order Hankel function of the second kind
$H_2^{(2)}()$	2nd order Hankel function of the second kind
I	area moment of inertia about the neutral axis
$[I]$	identity matrix
$Im\{\}$	imaginary part of the quantity inside the braces
j	square root of -1
k	wavenumber
k_η	translational stiffness of the boundary
k_θ	rotational stiffness of the boundary
K_η	dimensionless translational stiffness
K_θ	dimensionless rotational stiffness
m	mass per unit width for a beam, mass per unit area for a plate.
m_η	mass per unit length of the boundary
m_θ	rotational inertia per unit length of the boundary
M_h	bending moment per unit length in the direction of wave propagation
$M_{h'}$	bending moment per unit length perpendicular to the direction of wave propagation
M_p	amplitude (source strength) of a point moment input
M_t	twisting moment per unit length in the plate
p	loading function
P	amplitude of the loading function
Q	shear per unit length in the plate
Q_p	amplitude (source strength) of a quadrapole input
r	radial distance from the source

$[r]$ reflection matrix

$R_e\{\}$ real part of the quantity inside the braces

t time

x cartesian coordinate

y cartesian coordinate

w_x real power per unit length flowing in the x direction

w_y real power per unit length flowing in the y direction

w_{xb} bending component of the real intensity in x direction

w_{xs} shear component of the real intensity in x direction

w_{xt} twist component of the real intensity in x direction

w_{yb} bending component of the real intensity in y direction

w_{ys} shear component of the real intensity in y direction

w_{yt} twist component of the real intensity in y direction

∂ denotes partial differentiation

$\delta(\ )$ Dirac delta function

Δ transducer (finite difference) spacing

η transverse displacement of the beam or plate

η_i transverse displacement at location i on the on the beam or plate ($i = 1, 2, 3, \ldots 13$)

η' solution to the modified Bessel's equation

η solution to Bessel's equation

θ_b slope in the direction of wave propagation

θ_t angle of twist

ν Poisson's ratio

ξ_t translational damping ratio for the boundary

ξ_θ rotational damping ratio for the boundary

π ratio of circumference to the diameter of a circle

6

Π_x time averaged complex intensity in the x direction

ϕ azimuthal angle

ω radian driving frequency

∇^2 Laplacian operator

∇^4 Biharmonic operator

$\langle \cdot \rangle_t$ denotes a time average

$\approx$ approximately equal to

$\cdot$ differentiation with respect to time

$\cdot\cdot$ twice differentiation with respect to time

REVIEW OF THE FREE FIELD METHOD

The time averaged intensity (power flow per unit length) of transverse waves flowing in the x direction through a two dimensional structure is given by the equation

$$\Pi_x = \langle Q\dot\eta \rangle_t + \langle M_b\dot\theta_b \rangle_t + \langle M_t\dot\theta_t \rangle_t \tag{1}$$

where the individual terms in equation (1) are given by

$$\dot\eta = \frac{\partial\eta}{\partial t} \tag{2}$$

$$\theta_b = \frac{\partial\eta}{\partial x} \tag{3}$$

$$\theta_t = \frac{\partial\eta}{\partial y} \tag{4}$$

$$Q = B\frac{\partial}{\partial x}\left(\frac{\partial^2\eta}{\partial x^2} + \frac{\partial^2\eta}{\partial y^2}\right) \tag{5}$$

7

$$M_b = B\left[\frac{\partial^2 \eta}{\partial x^2} + \mu \frac{\partial^2 \eta}{\partial y^2}\right], \tag{6}$$

$$M_t - B(1 - \mu)\frac{\partial^2 \eta}{\partial x \partial y}. \tag{7}$$

Noiseux[1] has shown that equation (1) can be simplified considerably when the power flow takes place under free field conditions. In reference 1, it is shown that if there are no power sources or discontinuities in the properties of the media (boundaries) nearby, then the following relationship holds:

$$- M_b \dot{\theta}_b >_t + < M_t \dot{\theta}_t >_t \approx < \left[\frac{(M_b + M_{b\perp})}{(1 - \mu)}\right]\dot{\theta}_b >_t . \tag{8}$$

Further, it is shown in reference 1 that the approximation given by equation (8) can be easily obtained from measurable quantities under free field measurements conditions from the following relation:

$$\left[\frac{(M_b + M_{b\perp})}{(1 - \mu)}\right] \quad B\nabla^2 \eta \approx Bk^2 \eta. \tag{9}$$

Substituting the approximation of equation (9) into equation (1) the resulting equation for the total power flow is

$$\Pi_r \quad Q\dot{\eta} >_t + Bk^2 < \eta \dot{\theta}_b >_t . \tag{10}$$

Since the total power flow is shared equally by the shear and bending components under free field conditions, equation (10) can be reduced further to the following simple result:

$$\Pi . \quad 2Bk^2 \quad \eta \dot{\theta}_b >_t . \tag{11}$$

Equation (11) has been used by a number of researchers to obtain an estimate of the power flowing in simple beam and plate structures[1,6]. The most popular

8

experimental implementation of equation (11) utilizes two accelerometers and the following finite difference approximations:

$$\eta \approx |\eta_1 + \eta_2|/2. \tag{12}$$

$$\dot{\theta}_b \approx [\dot{\eta}_1 - \dot{\eta}_2]/\Delta. \tag{13}$$

Substituting equations (12) and (13) into equation (11) the result is

$$\Pi_r = \frac{Bk^2}{\Delta} \bullet [< \eta_1\dot{\eta}_1 >_t + < \eta_2\dot{\eta}_1 >_t - < \eta_1\dot{\eta}_2 >_t - < \eta_2\dot{\eta}_2) >_t]. \tag{14}$$

Expressing equation (14) in terms of acceleration rather than displacement and velocity, converting to the frequency domain and taking the real part of the result, the equation for intensity is

$$w_r = \frac{Bk^2}{(\omega^3\Delta)} \bullet Im\{|G_{11} - G_{22} + G_{21} - G_{12}|\} - \frac{2Bk^2}{(\omega^3\Delta)} Im\{G_{21}\}. \tag{15}$$

and since $k^4 = \omega^2 m/B$ the result can be written as

$$w_r = \frac{2(Bm)^{1/2}}{(\omega^2\Delta)} Im\{G_{21}\}. \tag{16}$$

Thus, equation (16) can be used as an estimate of the power flowing in a beam or plate using the two-accelerometer method.

THE DIRECT FINITE DIFFERENCE APPROACH

An alternate approach to the problem of measuring power flow in structures is to perform direct finite difference approximations of equations (2) through (7) by using a more sophisticated computational molecule. Consider the computational molecule shown in figure 1. This computational molecule consists of an array of 13 measurement transducers (accelerometers) arranged in a symmetric

fashion on a two dimensional surface (e.g. a plate). If each transducer in the molecule consists of a 0.3 gram accelerometer, the combined mass load on the surface of the structure amounts to 3.9 grams. (The mass load per unit area will depend on the tranducer spacing.) Other computational molecules with fewer transducers (e.g. 10 transducers[2]) can be used in the finite difference approach. The 13 transducer molecule, however, was chosen for study since it provides estimates of the power flow in the x and y directions at the same location in a 2 dimensional structure.

Utilizing the computational molecule of figure 1, the following central difference approximations can be made:

$$\ddot{\eta} \quad \frac{\partial}{\partial t}\dot{\eta} = \frac{\partial}{\partial t}\dot{\eta}_7, \tag{17}$$

$$\dot{\theta}_b \quad \frac{\partial}{\partial x}\dot{\eta} = \frac{(\dot{\eta}_3 \quad \dot{\eta}_{11})}{(2\Delta)}, \tag{18}$$

$$\dot{\theta}_t \quad \frac{\partial}{\partial y}\dot{\eta} = \frac{\dot{\eta}_6 + \dot{\eta}_8}{(2\Delta)}, \tag{19}$$

$$Q \quad B\frac{\partial}{\partial x}[\nabla^2\eta] = \frac{B}{2\Delta^3}[\eta_1 + \eta_2 \quad 4\eta_3 + \eta_4 \quad \eta_{10} + 4\eta_{11} \quad \eta_{12} \quad \eta_{13}], \tag{20}$$

$$M_b \quad B[\frac{\partial^2\eta}{\partial x^2} + \mu\frac{\partial^2\eta}{\partial y^2}] = \frac{B}{\Delta^2}[(\eta_3 \quad 2\eta_7 + \eta_{11}) + \mu(\eta_6 \quad 2\eta_7 + \eta_8)], \tag{21}$$

$$M_t \quad B(1 \quad \mu)\frac{\partial^2\eta}{\partial x\partial y} \quad \frac{B}{4\Delta^2}(1 \quad \mu)[\quad \eta_2 + \eta_4 + \eta_{10} \quad \eta_{12}], \tag{22}$$

These central difference approximations may be rewritten in terms of accelerations instead of displacements and substituted into the appropriate terms into equation (1). Converting this form of equation (1) to the frequency domain

10

and taking the real part of the result, it can be shown that the shear, bending, and twist components of the power flow are given respectively by

$$w_{xs} \approx \frac{B}{2\Delta^3\omega^3} \bullet [Im\{G_{17} + G_{27} - 4G_{37} + G_{47} - G_{107} + 4G_{117} - G_{127} - G_{137}\}], \quad (23)$$

$$w_{xb} \approx \frac{B}{2\Delta^3\omega^3} \bullet [Im\{(G_{33} - 2G_{73} + G_{113} - G_{311} + 2G_{711} - G_{1111}) \atop + \mu(G_{63} - 2G_{73} + G_{83} - G_{611} + 2G_{711} - G_{811})\}], \quad (24)$$

$$w_{xt} \approx B\frac{(1-\mu)}{(8\Delta^3\omega^3)} \bullet Im\{G_{26} - G_{46} - G_{106} + G_{126} - G_{28} + G_{48} + G_{108} - G_{128}\}, \quad (25)$$

Recalling the following properties of cross spectra

$$Im\{G_{\alpha\alpha}\} = 0, \quad (26)$$

$$Im\{G_{\beta\alpha}\} = -Im\{G_{\alpha\beta}\}, \quad (27)$$

it is seen that equations (23) through (25) require a total of 21 independent cross channel measurement pairs in order to compute estimates of the real part of the shear, bending, and twist components of the power flow. Thus, the experimental implementation of the computational molecule of figure 1 requires at least 2 passes with most 16 channel FFT analyzers, or 3 passes with most 8 channel FFT analyzers.

Finite difference approximations for the shear, bending, and twist components of the power flow in the y direction can be obtained in a similar fashion. The results of the derivations are given by the equations

$$w_{ys} \approx \frac{B}{2\Delta^3\omega^3} \bullet [Im\{-G_{27} + G_{47} - G_{57} + 4G_{67} - 4G_{87} - G_{97} - G_{107} - G_{127}\}], \quad (28)$$

11

$$w_{yb} \approx \frac{B}{2\Delta^3\omega^3} \bullet [Im\{(G_{68} - 2G_{78} + G_{88} - G_{86} + 2G_{76} - G_{66}) \tag{29}$$
$$+ \mu(G_{38} - 2G_{78} + G_{118} - G_{36} + 2G_{76} - G_{116})\}]$$

$$w_{yt} \approx B\frac{(1-\mu)}{(8\Delta^3\omega^3)} \bullet Im\{-G_{23} + G_{43} + G_{103} - G_{123} + G_{211} - G_{411} - G_{1011} + G_{1211}\}, \tag{30}$$

Equations (28) through (30) indicate that 13 additional independent cross channel measurement pairs are required to obtain the components of the real power flow in the y direction. Thus, the implementation of the computational molecule of figure 1 requires a total of 34 independent cross spectral measurements to obtain the six components of power flow in the x and y directions. In practice, this would require 3 passes with most 12 or 16 channel FFT analyzers, or 5 passes with most 8 channel analyzers.

It should also be noted that if the geometrical characteristics of the structure under investigation are 1 dimensional, the direct finite difference approach simplifys considerably. For example, if the structure is a simple beam, the equation for the power flow is given by

$$\Pi_x = Q\dot{\eta} + \cdots M_b\dot{\theta}_b \cdots, \tag{31}$$

For the case of the 1 dimensional structure, the central finite difference approximations for $\dot{\eta}$ and for $\dot{\theta}_b$ remain the same (see equations (17) and (18)). The formulae for the shear and bending moment simplify to the expressions

$$Q - EI\frac{\partial^3\eta}{\partial x^3} - EI - \eta_1 - 2\eta_8 + 2\eta_{11} - \eta_{13} \cdots \frac{}{(2\Delta^3)}, \tag{32}$$

$$M_b - EI\frac{\partial^2\eta}{\partial x^2} - EI - \eta_3 - 2\eta_7 + \eta_{11} \cdots \frac{}{\Delta^2}, \tag{33}$$

12

Thus, it is seen that only 5 of the 13 transducers are required in this case. Further analysis shows that the equations for the real parts of the shear and bending components of the power flow are given by

$$w_{\tau s} \approx \frac{EI}{(2\Delta^3\omega^3)} \bullet Im\{G_{17} - 2G_{37} + 2G_{117} - G_{137}\}, \tag{34}$$

$$w_{zb} \approx \frac{EI}{(2\Delta^3\omega^3)} \bullet Im\{G_{33} - 2G_{73} + G_{113} - G_{311} + 2G_{711} - G_{1111}\}, \tag{35}$$

Equations (34) and (35) indicate that only 5 independent cross spectral measurements must be performed in order to obtain estimates of the real part of the shear and bending components of the power flow in a beam. This requires a single pass with most multichannel FFT analyzers.

SIMULATED MEASUREMENTS

A series of analytical simulations of the two accelerometer and the direct finite difference measurement methods were performed in order to quantify and compare the accuracy of the two methods under near field measurement conditions. In the subsections that follow, selected results of the computer simulations of the two methods are presented for the cases of measurements in a plate near to a line force, a line moment, a point force, a point moment, and a quadrupole. Secondly, selected results are presented for simulated measurements near to boundaries which possess various combinations of mass, translational stiffness, rotational inertia, and rotational stiffness properties. (The geometrical arrangement of the input forcing function, the transducers, and the boundary are shown in figure 2.) A 0.32 cm thick AA2024 aluminum plate was chosen as the test vehicle for the simulations since it is representative of the materials and structural aspect ratios used in aircraft construction. The material properties of the plate are presented in Table I

Each data figure presented in the subsections that follow consists of parts (a) and (b). Part (a) shows the relative error of the two measurement methods in dB (relative to the known exact solution) over the 0 - 1000 Hz frequency range. Part (b) shows the intensity of the power flow in dB (relative to 1 Watt/meter) as estimated by the two measurement methods for a forcing function which has a uniform input over the 0 - 1000 Hz frequency range. In each case, the two figures viewed together provide some insights into the significance of the error. The results produced by the two accelerometer method are denoted by the words FREE FIELD and the results produced by the direct finite difference approach are denoted by the word DIRECT in both the figure legends and in the discussions that follow. The 0 - 1000 Hz frequency range was chosen for the analysis since it is of primary importance in propeller driven aircraft.

The exact solution for the structural intensity flowing in the plate for each flow field under examination was obtained in the following manner: The exact solutions for the transverse displacement, transverse velocity, angular velocity, rate of twist, shear, bending moment, and twisting moment as a function of position on the plate were derived. (Summaries of these analytical derivations are presented in Appendices I through III.) The results of these derivations were incorporated in the computer codes and were used in conjunction with equation (1) to calculate the exact amounts of structural intensity flowing in shear, bending, and twist at any location in the plate

The two measurement methods were simulated for each flow field under investigation as follows: The analytical result for the transverse displacement as a function of position on plate was utilized to compute the acceleration that would be experienced by each individual accelerometer in the transducer array. (The computed transverse displacement was multiplied by ω^2 in the frequency domain to obtain the acceleration in each case.) The computed accelerations were then

14

Each data figure presented in the subsections that follow consists of parts (a) and (b). Part (a) shows the relative error of the two measurement methods in dB (relative to the known exact solution) over the 0 - 1000 Hz frequency range. Part (b) shows the intensity of the power flow in dB (relative to 1 Watt/meter) as estimated by the two measurement methods for a forcing function which has a uniform input over the 0 - 1000 Hz frequency range. In each case, the two figures viewed together provide some insights into the significance of the error. The results produced by the two accelerometer method are denoted by the words FREE FIELD and the results produced by the direct finite difference approach are denoted by the word DIRECT in both the figure legends and in the discussions that follow. The 0 - 1000 Hz frequency range was chosen for the analysis since it is of primary importance in propeller driven aircraft.

The exact solution for the structural intensity flowing in the plate for each flow field under examination was obtained in the following manner: The exact solutions for the transverse displacement, transverse velocity, angular velocity, rate of twist, shear, bending moment, and twisting moment as a function of position on the plate were derived. (Summaries of these analytical derivations are presented in Appendices I through III) The results of these derivations were incorporated in the computer codes and were used in conjunction with equation (1) to calculate the exact amounts of structural intensity flowing in shear, bending, and twist at any location in the plate.

The two measurement methods were simulated for each flow field under investigation as follows: The analytical result for the transverse displacement as a function of position on plate was utilized to compute the acceleration that would be experienced by each individual accelerometer in the transducer array. (The computed transverse displacement was multiplied by ω^2 in the frequency domain to obtain the acceleration in each case.) The computed accelerations were then

substituted into the finite difference approximations utilized by each measurement method. Thus, a 4 transducer computational molecule was used in conjunction with equations (12) and (13) to simulate the two accelerometer method while a 13 transducer computational molecule was used in conjunction with equations (18) through (23) to simulate the direct finite difference approach.

A 2 cm transducer spacing was selected for the two accelerometer method while a 1 cm transducer spacing was selected for the direct finite difference approach. It is acknowledged at the outset that these choices provide the direct approach with a slight advantage over the two accelerometer approach in the high frequency ranges (beyond the scope of analysis of this paper) where finite difference error is important. In the low frequency ranges where near field error is important, however, the larger transducer spacing for the two accelerometer probe should, if anything, provide it with a slight advantage over the direct approach.

MEASUREMENTS NEAR A LINE FORCE

Figures 3 and 4 show typical results obtained for simulated measurements in a plate near to a line force input. A summary of the analysis used to generate these results is given in Appendix I. The amplitude of the line force disturbance was fixed at 10.0 N/m.

For the case shown in figure 3, the geometric center of each measurement probe is located at a distance of 10 cm from the line force discontinuity (31.5 times the thickness of the plate). Figure 3(a) indicates that the near field error for the FREE FIELD method is less than 1 dB everywhere except in the frequency range below 50 Hz. The near field error of the DIRECT method is seen to be negligible in all frequency ranges. Figure 3(b) adds additional insight into figure 3(a) since it indicates that the frequency range in which the FREE FIELD method experiences the largest errors coincides with the frequency range of maximum

15

power flow for a uniform input force. Thus, the error in the estimates produced by the FREE FIELD method can be significant in some cases. (Note: References 4, 5, and 6 present results similar to those shown in figure 3(a) for the case of a line force input, but do not include the accompanying plot of the intensity of the power flow.)

Figure 4 shows the results obtained when the measurement probes are located 5 cm from the line force discontinuity (15.75 times the plate thickness). These results indicate that the magnitude of the error in the intensity estimates produced by the FREE FIELD method increases in the lower frequency ranges. The estimates produced by the DIRECT method remains very accurate, however. Also, from comparison of figures 3 and 4, it can be seen that the errors produced by the free field approximations will change sign in some frequency ranges when the probe is moved closer to the input. Thus, the FREE FIELD method may either overestimate or underestimate the true intensity depending on the location of the measurement probe.

MEASUREMENTS NEAR A LINE MOMENT

Figure 5 shows typical results obtained for simulated measurements in a plate near to a line moment input. The analysis used to generate these results is summarized in Appendix I. The amplitude of the line moment disturbance was fixed at 0.20 Nm/m. For the case shown in figure 5, each measurement probe is located 10 cm from the line moment discontinuity. In this case, the near field error in the estimates produced by the FREE FIELD method is seen to be consistently negative (the true intensity is underestimated) and the errors are larger in magnitude than those experienced when measuring near a line force (see figure 4). The near field error of the estimates produced by the DIRECT method in figure 5 is negligible by comparison. These results are in sharp contrast to the results of figures 3 and 4 where the error curve produced by the FREE FIELD method "hovers"

16

about the axis of 0 error. In fairness to the FREE FIELD approach, however, it should be noted that the frequency range in which large error occurs in its estimates coincides with the frequency range of minimum power flow for a uniform line moment input.

MEASUREMENTS NEAR A POINT FORCE

The two methods of power flow measurement were also simulated for the case of measurement near a uniform point force input to an infinite plate. The magnitude of the point driving force input was fixed at 10.0 N. Qualitatively, the results obtained for these simulations were very similar to those obtained for a line force input (See figures 3 and 4.). This is to be expected since the solutions to this type of flow field (summarized in Appendix II) must obey the radial symmetry of the problem. Therefore, the results obtained should exhibit similar one dimensional type behavior.

The simulations for the point force did produce one notable addition to the previous body of knowlege, however. For the case shown in figure 6, each measurement probe is located 5 cm from the point force discontinuity. In figure 6(a), the error curve for the FREE FIELD method does not cross the axis of 0 error, but underestimates the true intensity over the entire frequency range of interest. (In other cases where the measurement probes are 10 cm or further from the source, the error curve of the FREE FIELD method crosses the 0 error axis.) Thus, unlike the results obtained for the line force, the error curve of the FREE FIELD method does not necessarily "hover" about the axis of 0 error. Since the amount of power input to the plate is uniform over the entire frequency range in this case (see figure 6(b)), the large near field error introduced by the FREE FIELD method at low frequency could significantly degrade the accuracy of the estimate of the total power flow. Also note that the near field error experienced

17

by the DIRECT method of measurement is once again insignificant in comparison to that experienced by the FREE FIELD method.

MEASUREMENTS NEAR A POINT MOMENT

Figures 7 and 8 show typical results obtained (using the analysis summarized in Appendix II) for simulated measurements in a plate near to a point moment input. The amplitude of the point moment was fixed at 0.20 Nm. Unlike the results presented for the previous cases, the flow field in this case possesses a strong directional character.

For example, figure 7 shows the results of the simulations when each measurement probe is located 10 cm from the point moment and aligned along the dipole axis (ϕ 0 degrees). (The flow field of a point moment can be mathematically represented as a force couple or dipole.) In this case, the near field error in the estimates produced by the FREE FIELD method is consistently negative, but is unacceptably large only at frequencies below 200 Hz. The DIRECT method is seen to produce very accurate estimates by comparison.

As the measurement probes are moved either radially inward (closer to the source), or moved circumferentially in the azimuthal angle ϕ, the performance of the FREE FIELD method is seriously degraded. For example, figure 8 shows the results of the simulations when each measurement probe is located at an azimuthal angle ϕ of 80 degrees. The measurement probes are again directed at the point moment source and located at a distance of 10 cm away. Thus, the results of figure 8 are for the measurement of intensity along an axis that is almost in pure twist. These results indicate that the estimates produced by the FREE FIELD method along this axis are so inaccurate that no useful information can be obtained from them. In contrast, the estimates produced by the DIRECT method remain accurate across the entire 0-1000 Hz frequency range.

18

MEASUREMENTS NEAR A QUADRUPOLE SOURCE

Figures 9 and 10 show typical results obtained (using the analysis summarized in Appendix II) for simulated measurements in a plate near to a lateral quadrupole input. The amplitude of the quadrupole was fixed at 0.02 Nm^2. The case of the lateral quadrupole is of interest since its flow field closely resembles that of a point force input located near the corner of a semi-infinite plate which is simply supported along its two edges.

Figure 9 shows the results of the simulations when each of the measurement probes is directed at the quadrupole source located 10 cm away. In this case, the azimuthal angle ϕ was fixed at 45 degrees. This should be the best case scenerio for FREE FIELD measurement accuracy since the axis along the 45 degree azimuth is the axis of minimum twist. The near field error in the estimates produced by the FREE FIELD method is consistently negative and significant at frequencies below 300 Hz. The DIRECT method is seen to produce very accurate estimates over the entire frequency range.

Once again, as the measurement probes are moved either radially inward, or moved circumferentially, the performance of the FREE FIELD method is seriously degraded. Figure 10 shows the results of the simulations when each of the measurement probes is located at an azimuthal angle ϕ of 10 degrees. The probes are again directed at the quadrupole source and located at a distance of 10 cm away. The estimates produced by the FREE FIELD method along this axis are grossly inaccurate. The estimates produced by the DIRECT method, however, remain accurate across the entire frequency range.

MEASUREMENTS NEAR A LINE BOUNDARY
WITH MASS AND TRANSLATIONAL STIFFNESS

Figures 11 and 12 show typical results obtained from the simulations for measurements in a plate near to a line boundary which possesses a translational

stiffness k_η of 1.0×10^7 N/m/m, a mass m_η of 1.0 kg/m, and a viscous critical damping ratio ζ_η of 0.01. A summary of the analysis used to generate the results is given in Appendix III. The analysis utilizes a uniform line force input of 10.0 N/m amplitude located 1 m away from the boundary to generate incident traveling waves on the boundary (see figure 2). The numerical values chosen to characterize the boundary and the input forcing function are somewhat arbitrary but representative of typical values that might be encountered in existing aircraft type structures. The large distance between the source and the boundary insures that the boundary does not experience any near field effects associated with the source. Thus, the boundary "sees" only incident propagating waves.

For the case shown in figure 11, the measurement probes are located 10 cm away from the boundary. Figure 11(a) indicates that the near field error for the FREE FIELD method is less than 1 dB everywhere except in the frequency range below 300 Hz. The DIRECT method is seen to be accurate over the entire frequency range. Figure 11(b) indicates that the frequency ranges of largest error and maximum power flow coincide for the FREE FIELD method. Thus, the error in the estimates produced by the FREE FIELD method can be significant. Also note that very little power flows through the boundary in the vicinity of 300 Hz. This phenomenon is caused by the strong impedance mismatch effects of the boundary at this frequency. It can be shown that the exact location (in frequency) of the impedance mismatch is dependent primarily on the value of the stiffness of the boundary k_η.

Figure 12 shows the results obtained when the measurement probes are located 5 cm from the boundary. Figure 12(a) indicates that the magnitude of the error in the intensity estimates produced by the FREE FIELD method increases as the transducers are moved closer to the boundary. The estimates produced by the DIRECT

method remain very accurate, however. Figure 12(b) is plot of the absolute values of the intensity estimates for the two methods. It is important to note that the FREE FIELD method produces negative intensity values in the 175 - 275 Hz frequency range. Thus, the FREE FIELD method indicates that the power is flowing out of the boundary rather than through the boundary in this frequency range.

MEASUREMENTS NEAR A LINE BOUNDARY WITH ROTATIONAL STIFFNESS AND INERTIA

Figures 13 and 14 show typical results obtained (using the analysis of Appendix III) from the simulations of measurements in a plate near to a line boundary which possesses a rotational stiffness k_θ of 1.0×10^3 N-m/m, a rotational mass moment of inertia m_θ of 0.001 kg-m^2/m, and a viscous critical damping ratio ξ_θ of 0.01. The analysis utilizes a uniform line force input of 10.0 N/m amplitude located 1 m away from the boundary to generate incident traveling waves on the boundary (see figure 2). Once again, the numerical values chosen to characterize the boundary and the input forcing function are arbitrary but realistic values. The large distance between the source and the boundary insures that the boundary does not experience any near field effects associated with the source.

For the case shown in figure 13, the measurement probes are located 10 cm away from the boundary. Figure 13(a) indicates that the near field error for the FREE FIELD method is acceptable over the entire frequency range. The DIRECT method is seen to be slightly more accurate than the FREE FIELD method. Also note that very little power flows through the boundary in the vicinity of 850 Hz. Thus, the impedance mismatch phenomenon occurs at a much higher frequency in this case. It can be shown that the location of the impedance mismatch is dependent primarily on the value of the rotational inertia of the boundary m_θ.[8]

Figure 14 shows the results obtained when the measurement probes are located 5 cm from the boundary. Figure 14(a) indicates that the magnitude of the error

in the intensity estimates produced by the FREE FIELD method greatly increases at frequencies above 500 Hz. The estimates produced by the DIRECT method remain very accurate, however. Figure 14(b) is plot of the absolute values of the intensity estimates for the two methods. Note that the FREE FIELD method produces negative intensity values in the vicinity of 800 Hz indicating that the power is flowing out of rather than through the boundary in this range. Therefore, the accuracy of the FREE FIELD method can not necessarily be guaranteed in the higher frequency ranges, but may depend on the location of the transducers and the characteristics of the boundary.

MEASUREMENTS NEAR A LINE BOUNDARY WITH TRANSLATIONAL AND ROTATIONAL PROPERTIES

Figures 15 and 16 show typical results obtained (using the analysis of Appendix III) for the simulations of measurements in a plate near to a line boundary which possesses both the translational and rotational stiffness and inertia properties discussed in the two previous subsections

$$(k_{\eta} \quad 1.0 + 10^7 \ N/m/m, \ m_{\eta} \quad 1.0 \ kg/m, \ \xi_{\eta} \quad 0.01 ,$$
$$k_{\theta} \quad 1.0 \cdot 10^5 \ N\text{-}m/m, \ m_{\theta} \quad 0.001 \ kg\text{-}m^2/m, \ and \ \xi_{\theta} \quad .01) .$$

The analysis utilizes a uniform line force input of 10.0 N/m amplitude located 1 m away from the boundary to generate incident traveling waves on the boundary (see figure 2).

Figure 15 shows the results obtained when the measurement probes are located 10 cm away from the boundary. These results bear a strong resemblance to those obtained in figure 11. Figure 15(a) indicates that the near field error for the FREE FIELD method is less than 1 dB everywhere except in the frequency range of maximum power flow. The DIRECT method is seen to be accurate over the entire frequency range. Figure 15(b) suggests that the added rotational properties of

22

the boundary cause a secondary impedance mismatch at some frequency above 1000 Hz.

Figure 16 shows the results obtained when the measurement probes are located 5 cm from the boundary. The error curve of figure 16(a) indicates that the intensity estimates produced by the FREE FIELD method are inaccurate over the entire 0-1000 Hz frequency range. The estimates produced by the DIRECT method remain accurate, however. Figure 16(b) shows that the intensity estimates produced by the FREE FIELD method have the wrong sign near the first impedance mismatch (200-300 Hz) and deteriorate rapidly as they approach the second impedance mismatch (above 1000 Hz). Thus, it may be concluded that the magnitude and character of the near field error produced by the FREE FIELD method may depend on the particular combination of the translational and rotational properties of a boundary in the vicinity of the measurement probe.

MEASUREMENTS UNDER SEVERE, COMBINED NEAR FIELD CONDITIONS

Figures 17 shows typical results obtained (using the analysis of Appendix III) for the simulations of measurements in a plate with the measurement probes "sandwiched" between a line force and a line boundary. The boundary in this case possesses the properties discussed previously

$$(k_q \quad 1.0 \cdot 10^7 \text{ N/m/m}, \ m_q \quad 1.0 \text{ kg/m}, \ \xi_q \quad 0.01 ,$$

$$k_\theta \quad 1.0 \cdot 10^3 \text{ N-m/m}, \ m_\theta \quad 0.001 \text{ kg-m}^2/\text{m}, \text{ and } \xi_\theta \quad .01).$$

and is located 5 cm from the measurement probes. A line force input of uniform 10.0 N/m magnitude is positioned 10 cm from the boundary. Thus, the distance between the input and the geometric center of the transducers is also 5 cm.

Under these conditions, the transducers are affected by the propagating and evanescent components of both the input and the boundary. Furthermore, both the propagating and evanescent components of the reflections from the

23

boundary are altered by the presence of the near field component of the input. This modified response of the boundary is included in the analysis as outlined by Appendix III. It is assumed, however, that the flow field produced by the line force input is not altered by the presence of the boundary. (In practice, this would not be the case since the impedance "seen" by the input would change due to the close proximity of the boundary.) This simplification can be thought of as an alteration of the forcing function such that the characteristics of the flow field associated with the input remain the same.

Figure 17 shows that intensity estimates of the FREE FIELD method are negative (and therefore unusable) below 400 Hz. Interestingly, the accuracy of the FREE FIELD method actually improves in the 400-900 Hz range (compared to figure 16) due to the close proximity of the source. Above 900 Hz, the FREE FIELD estimates rapidly degenerate as they approach the secondary impedance mismatch. In contrast, the DIRECT method is seen to be accurate over the entire frequency range. Thus, it may be concluded that the magnitude and character of the near field error associated with the FREE FIELD measurement method may also depend on the combined characteristics of the sources and boundaries in the vicinity of the measurement probe.

CONCLUDING REMARKS

Overall, the results of the study indicate that the near field error associated with the FREE FIELD (two accelerometer) measurement method is much more serious than previously believed.

Simulations of FREE FIELD measurements near to simple sources show that the error curve of this method does not necessarily "hover" about the axis of 0 error as implied by the more limited results presented in references 4, 5, and 6. Furthermore, it was shown that the frequency range of maximum error often coincides with the frequency range of maximum power flow when measuring

24

near simple sources. It was shown that both the sign and the magnitude of the near field error associated with the FREE FIELD method is very sensitive to the distance between the measurement probe and the source. And it was shown that the accuracy of the FREE FIELD method is highly dependent on the radial and azimuthal location of the measurement probe (with respect to the source) when measuring near higher order sources (dipoles and quadrupoles).

Simulations of FREE FIELD measurements near to simple boundaries show that this method can actually indicate that the intensity is flowing in the wrong direction. Furthermore, it was shown that this type of error is not necessarily restricted to the lower frequency ranges and can occur in frequency ranges where the power flow is relatively large and stable.

The results of the simulations for the DIRECT method are in sharp contrast to the results obtained for the FREE FIELD method. In essentially all cases under investigation (all simple sources and boundaries studied) the direct finite difference approach produced an accurate estimate of the intensity flowing in the plate. The estimates produced by this method were so accurate, in fact, that no significant difference was found between the estimates and the exact solution for any near field measurement condition studied.

In fairness to the FREE FIELD approach it should be noted that many of the serious near field errors inherent in the method can be suppressed for a given measurement condition by increasing the spacing between the two accelerometers. Using this technique, the near field effects can be "shifted" to the very low frequency ranges (beyond the range of interest). This solution is not a panacea, however, since it will also cause the error associated with the finite diff· ence approximations to greatly increase in significance.

It should also be noted that the FREE FIELD approach may be quite useful for obtaining estimates of the power flow in situations where there are no sources

25

nearby, or in situations where the properties of the structure do not change in the vicinity of the measurement probe.

Lastly, it should be pointed out that both methods are subject to other types of measurement error. Quinlin[4] and Redman-White[5] have shown that the FREE FIELD method has difficulty producing an accurate estimate of the structural intensity in reverberant flow fields. Furthermore, Mickol's results[6] suggest that the presence of the measurement probe itself can significantly alter the flow field and therefore degrade the accuracy of the measurements. It is expected that the DIRECT method suffers from similar adverse effects.

APPENDIX I

EQUATIONS FOR THE TRANSVERSE VIBRATION OF AN INFINITE BEAM

General Solution for a Discrete Forcing Function

The governing differential equation for the transverse vibration of an infinite beam is given by (see reference 7)

$$B\nabla^4 \eta + m\frac{\partial^2 \eta}{\partial t^2} = p(x,t). \tag{A.1}$$

If it assumed that the forcing function is simple harmonic in character and occurs at a discrete location in space, i.e.

$$p(x,t) = P\delta(x)e^{i\omega t}, \tag{A.2}$$

then the resulting motion of the beam is also simple harmonic and the governing equation becomes

$$\left(\nabla^4 - \frac{m\omega^2}{B}\right)\eta = \frac{P}{B}\delta(x)e^{i\omega t}. \tag{A.3}$$

Now for the case of an infinite beam

$$\nabla^4 = \frac{d^4}{dx^4}, \tag{A.4}$$

and defining $k^4 = m\omega^2/B$, the governing equation becomes

$$\frac{d^4 \eta}{dx^4} - k^4 \eta = \frac{P}{B}\delta(x)e^{i\omega t}. \tag{A.5}$$

For values of $x \neq 0$, the governing equation is:

$$\frac{d^2}{dx^2}\left(k^2 \eta + \frac{d^2 \eta}{dx^2}\right) - k^4 \eta = 0. \tag{A.6}$$

This linear ordinary homogeneous differential equation is easily solved using operator methods and the solution is given by

$$\eta(r,t) = [C_1 e^{-jkr} + C_2 e^{jkr} + C_3 e^{-kr} + C_4 e^{kr}] e^{j\omega t}, \tag{A.7}$$

for values of $r > 0$. Furthermore, from physical considerations, the value of η must remain finite as r approaches infinity. Therefore, $C_4 = 0$ and since all waves propagate away from the source, $C_2 = 0$ for values of $r > 0$. Thus, the solution becomes

$$\eta(r,t) = [C_1 e^{-jkr} + C_3 e^{-kr}] e^{j\omega t}, \tag{A.8}$$

for values of $r > 0$.

Solution for a Point Force Input

For the case of a discrete point force of amplitude F_p located at $r = 0$ on an infinite beam, the following two boundary conditions apply:

$$\frac{\partial \eta}{\partial r}(r = 0) = 0, \tag{A.9}$$

$$Q(r = 0) = B \frac{\partial^3 \eta}{\partial r^3}(r = 0) = \frac{F_p}{2} \tag{A.10}$$

Applying the boundary condition of equation (A.9) to the solution given by equation (A.8), it can be shown that

$$C_3 = j C_1 \tag{A.11}$$

Thus the solution reduces to

$$\eta(r,t) = C_1 [e^{-jkr} + j e^{-kr}] e^{j\omega t} \tag{A.12}$$

28

Applying the boundary condition of equation (A.10) to the solution given by (A.12), it is found that

$$C_1 = \frac{jF_p}{(4Bk^3)},\qquad (A.13)$$

and the solution for the transverse displacement for $x = 0$ as a function of time is given by

$$\eta(x,t) = \frac{jF_p}{(4Bk^3)}\left[e^{-jkx} - je^{-kx}\right]e^{j\omega t}.\qquad (A.14)$$

Differentiating with respect to time to obtain the transverse velocity for $x = 0$,

$$\dot{\eta}(x,t) = \frac{\omega F_p}{(4Bk^3)}\left[e^{-jkx} - je^{-kx}\right]e^{j\omega t}.\qquad (A.15)$$

The angular velocity for $x = 0$ is found by differentiating equation (A.15) with respect to x. Thus

$$\frac{\partial\eta}{\partial x} = \frac{j\omega F_p}{(4Bk^2)}\left[e^{-jkx} - e^{-kx}\right]e^{j\omega t}.\qquad (A.16)$$

The moment in the beam for $x = 0$ as a function of time can be obtained by differentiating equation (A.14) twice with respect to x. The result is

$$M(x,t) = B\frac{d^2\eta}{dx^2} = \frac{jF_p}{(4k)}\left[e^{-jkx} + je^{-kx}\right]e^{j\omega t}.\qquad (A.17)$$

The shear in the beam for $x = 0$ can similarly be obtained from the third order differentiation of (A.14) with respect to x as follows:

$$Q(x,t) = B\frac{d^3\eta}{dx^3} = \frac{F_p}{4}\left[e^{-jkx} + e^{-kx}\right]e^{j\omega t}.\qquad (A.18)$$

29

Solution for a Point Moment Input

For the case of a discrete point moment of amplitude M_p located at $x = 0$ on an infinite beam, the following two boundary conditions apply:

$$\eta(x = 0) = 0, \tag{A.19}$$

$$M_b(x = 0) = B\frac{\partial^2\eta}{\partial x^2}(x = 0) = M_p/2. \tag{A.20}$$

Applying the boundary condition of equation (A.19) to the solution given by equation (A.8), it can be shown that

$$C_3 = C_1. \tag{A.21}$$

Thus the solution reduces to

$$\eta(x,t) = C_1[e^{jkx} - e^{-kx}]e^{j\omega t}. \tag{A.22}$$

Applying the boundary condition of equation (A.20) to the solution given by (A.22), it is found that

$$C_1 = \frac{M_p}{(4Bk^2)}, \tag{A.23}$$

and the solution for the transverse displacement for $x = 0$ as a function of time is given by

$$\eta(x,t) = \frac{M_p}{(4Bk^2)}[e^{jkx} - e^{-kx}]e^{j\omega t}. \tag{A.24}$$

Differentiating with respect to time to obtain the transverse velocity for $x = 0$,

$$\eta(r,t) = \frac{j\omega M_p}{(4Bk^2)}[e^{jkx} - e^{-kr}]e^{j\omega t}. \tag{A.25}$$

The angular velocity for $r > 0$ is found by differentiating equation (A.25) with respect to r. Thus

$$\frac{\partial \eta}{\partial r} = \frac{j\omega M_p}{(4Bk)}[je^{jkr} + e^{-kr}]e^{j\omega t}. \tag{A.26}$$

The moment in the beam for $r > 0$ as a function of time can be obtained by differentiating equation (A.24) twice with respect to r. The result is

$$M_b(r,t) = B\frac{\partial^2 \eta}{\partial r^2} = \frac{M_p}{1}[e^{jkr} + e^{-kr}]e^{j\omega t}. \tag{A.27}$$

The shear in the beam for $r > 0$ can similarly be obtained from the third order differentiation of (A.24) with respect to r as follows:

$$Q(r,t) = B\frac{\partial^3 \eta}{\partial r^3} = \frac{kM_p}{1}[je^{jkr} + e^{-kr}]e^{j\omega t}. \tag{A.28}$$

APPENDIX II

EQUATIONS FOR THE TRANSVERSE VIBRATION OF AN INFINITE PLATE

Governing Differential Equation for a Point Force

The governing differential equation for the transverse vibration of an infinite plate is given by (see reference 7)

$$B\nabla^4\eta + m\frac{\partial^2\eta}{\partial t^2} = p(r,\phi,t). \tag{A.29}$$

If it assumed that the forcing function is a simple harmonic force which occurs perpendicular to the plate at a discrete point in space, i.e.

$$p(r,\phi,t) = P\delta(r)e^{j\omega t}, \tag{A.30}$$

then the resulting motion of the plate is also simple harmonic and the governing equation becomes

$$\left(\nabla^4 - \frac{m\omega^2}{B}\right)\eta = \frac{P}{B}\delta(r)e^{j\omega t}. \tag{A.31}$$

Defining $k^4 = m\omega^2/B$, this becomes

$$(\nabla^4 - k^4)\eta = \frac{P}{B}\delta(r)e^{j\omega t}. \tag{A.32}$$

For values of $r \neq 0$, the governing equation is

$$(\nabla^4 - k^4)\eta = 0. \tag{A.33}$$

Since a point force produces a symmetric response in the variable r, there can be no ϕ dependence in the response η. Therefore, the Laplacian operator in this case reduces to

32

$$\nabla^2 - \frac{\partial^2}{\partial r^2} + \frac{1}{r}\frac{\partial}{\partial r}, \tag{A.34}$$

and the biharmonic operator is given by

$$\nabla^4 \quad \nabla^2\nabla^2. \tag{A.35}$$

Substituting this last result, the governing equation becomes

$$(\nabla^2 - k^2)(\nabla^2 + k^2)\eta = 0. \tag{A.36}$$

Solution for a Point Force

Equation (A.36) is a linear ordinary homogeneous differential equation. Using operator methods, this equation is easily solved. The solution is given by

$$\eta \quad \eta + \eta^* e^{i\omega t}, \tag{A.37}$$

where η must satisfy

$$\left(\frac{\partial^2}{\partial r^2} + \frac{1}{r}\frac{\partial}{\partial r} \quad k^2\right)\eta \quad 0, \tag{A.38}$$

and where η^* must satisfy

$$\left(\frac{\partial^2}{\partial r^2} + \frac{1}{r}\frac{\partial}{\partial r} + k^2\right)\eta^* \quad 0, \tag{A.39}$$

for values of $r \quad 0$.

Equations (A.38) and (A.39) are alternate forms of the ordinary and modified Bessel's equation of 0th order, respectively. The solutions to these two equations are well known and are given, respectively, by

$$\eta \quad C_1 H_0^{(1)}(kr) + C_2 H_0^{(2)}(kr), \tag{A.40}$$

33

$$\eta^+ \quad C_3 H_0^{(1)}(\ jkr) + C_4 H_0^{(2)}(-jkr), \tag{A.41}$$

where $H_0^{(1)}(\cdot)$ is the 0th order Hankel function of the 1st kind and $H_0^{(2)}(\cdot)$ is the 0th order Hankel function of the 2nd kind.

It can be shown (see reference 7) that $H_0^{(1)}(kr)$ corresponds to an inward travelling wave and that $H_0^{(1)}(-jkr)$ corresponds to a solution that grows exponentially without bound in kr. Therefore, from physical considerations, the coefficients of these two terms must be zero. Thus, the solution becomes

$$\eta(r,t) - [C_2 H_0^{(2)}(kr) + C_4 H_0^{(2)}(-jkr)]e^{j\omega t}, \tag{A.42}$$

where $H_0^{(2)}(kr)$ corresponds to an outward travelling wave and $H_0^{(2)}(\ jkr)$ corresponds to an exponently decaying solution in kr.

Applying the boundary condition

$$\lim_{(r \to 0)} \frac{\partial \eta}{\partial r} \quad 0, \tag{A.43}$$

(from symmetry considerations) to the solution given by (A.42), it is found that $C_4 \quad C_2$. Thus, the solution is reduced to

$$\eta(r,t) \quad C_2[H_0^{(2)}(kr) \quad H_0^{(2)}(\ jkr)]e^{j\omega t}. \tag{A.44}$$

Now from reference 7, the equation for the shear in the plate is given by the equation

$$Q \quad B \frac{\partial}{\partial r}(\nabla^2 \eta). \tag{A.45}$$

Applying the boundary condition

$$\lim_{(r \to 0)} Q \quad \frac{F_p}{(2\pi r)}, \tag{A.46}$$

34

it is shown in reference 7 that the value of C_2 is given by

$$C_2 = \frac{jF_p}{(8Bk^2)}. \tag{A.47}$$

Thus, the final solution for the displacement of the point driven infinite plate is given by

$$\eta(r,t) = \frac{jF_p}{(8Bk^2)}[H_0^{(2)}(kr) - H_0^{(2)}(-jkr)]e^{j\omega t}. \tag{A.48}$$

Equations for transverse velocity, angular velocity, bending moment, and shear can be obtained, respectively, by straightforward differentiation of equation (A.48) using the following formulae:

$$\dot{\eta} = \frac{\partial \eta}{\partial t} = j\omega\eta, \tag{A.49}$$

$$\dot{\theta}_b = \frac{\partial}{\partial t}\frac{\partial \eta}{\partial r} = j\omega k\frac{\partial \eta}{\partial(kr)}, \tag{A.50}$$

$$M_b = B[\frac{\partial^2 \eta}{\partial r^2} + \mu(\frac{1}{r}\frac{\partial \eta}{\partial r})], \tag{A.51}$$

$$Q = B\frac{\partial}{\partial r}(\nabla^2 \eta) = B\frac{\partial}{\partial r}(\frac{\partial^2 \eta}{\partial r^2} + \frac{1}{r}\frac{\partial \eta}{\partial r}). \tag{A.52}$$

Carrying out the operations indicated in equations (A.49) through (A.52), the equations for transverse velocity, angular velocity, bending moment, and shear for the case of an infinite plate driven by a point force are given, respectively, by:

$$\dot{\eta} = \frac{\omega F_p}{(8Bk^2)}[H_0^{(2)}(kr) - H_0^{(2)}(-jkr)]e^{j\omega t}, \tag{A.53}$$

$$\dot{\theta}_b = \frac{\omega F_p}{(8Bk)}[H_1^{(2)}(kr) + jH_1^{(2)}(-jkr)]e^{j\omega t}, \tag{A.54}$$

$$M_b = \frac{jF_p}{8}\left[H_0^{(2)}(kr) - H_0^{(2)}(-jkr) - \frac{(1-\mu)}{(kr)}[H_1^{(2)}(kr) + jH_1^{(2)}(-jkr)]\right]e^{j\omega t}, \tag{A.55}$$

$$Q = \frac{jkF_p}{8}[-H_1^{(2)}(kr) + jH_1^{(2)}(-jkr)]e^{j\omega t} \tag{A.56}$$

35

Solution for a Point Moment

The solution for an infinite plate driven by a simple harmonic point moment can be obtained directly from the solution for a point force by simple differentiation with respect to the cartesian coordinate x (see reference 7). Thus, the solution for the transverse displacement due to a point moment is given by

$$\eta = \frac{\partial}{\partial x} - \frac{jM_p}{(8Bk^2)}[H_0^{(2)}(kr) - H_0^{(2)}(-jkr)]e^{j\omega t}, \qquad (A.57)$$

and from the calculus it is known that

$$\frac{\partial}{\partial x} - \cos\phi \frac{\partial}{\partial r} - \frac{\sin\phi}{r}\frac{\partial}{\partial \phi}.$$

Since the monopole solution contains no ϕ dependence, the dipole (point moment) solution is given by

$$\eta - \frac{jM_p}{(8Bk)}\cos\phi\, e^{j\omega t} \cdot \frac{\partial}{\partial(kr)}[H_0^{(2)}(kr) - H_0^{(2)}(-jkr)].$$

Performing the indicated operation, the result is

$$\eta - \frac{jM_p}{(8Bk)}\cos\phi\,[H_1^{(2)}(kr) - jH_1^{(2)}(-jkr)]e^{j\omega t}, \qquad (A.58)$$

Note that this solution for the transverse displacement of the plate depends on both the radial distance r, and the azimuthal angle ϕ. Therefore, the power flow field due to a point moment input is not radially symmetric, and the flow field contains a component due to twist in addition to the ordinary shear and bending components.

Equations for transverse velocity, angular velocity, rate of twist, bending moment, shear, and twisting moment can be obtained, respectively, by straight-forward differentiation of equation (A.58) using the following formulae:

36

$$\dot{\eta} = \frac{\partial \eta}{\partial t} = j\omega\eta, \tag{A.59}$$

$$\dot{\theta}_b = \frac{\partial}{\partial t}\frac{\partial \eta}{\partial r} = j\omega k\frac{\partial}{\partial(kr)}\eta, \tag{A.60}$$

$$\dot{\theta}_t = \frac{\partial}{\partial t}\frac{1}{r}\frac{\partial \eta}{\partial \phi} = \frac{j\omega k}{(kr)}\frac{\partial}{\partial \phi}\eta, \tag{A.61}$$

$$M_b = B\left[\frac{\partial^2 \eta}{\partial r^2}\right] + B\mu\left[\frac{1}{r}\frac{\partial \eta}{\partial r} + \frac{1}{r^2}\frac{\partial^2 \eta}{\partial \phi^2}\right], \tag{A.62}$$

$$Q = B\frac{\partial}{\partial r}(\nabla^2 \eta) = B\frac{\partial}{\partial r}\left[\frac{\partial^2 \eta}{\partial r^2} + \frac{1}{r}\frac{\partial \eta}{\partial r} + \frac{1}{r^2}\frac{\partial^2 \eta}{\partial \phi^2}\right]. \tag{A.63}$$

$$M_t = B(1 - \mu)\left[\frac{1}{r}\frac{\partial^2 \eta}{\partial r\partial \phi} - \frac{1}{r^2}\frac{\partial \eta}{\partial \phi}\right]. \tag{A.64}$$

Carrying out the operations indicated in equations (A.59) through (A.64), the equations for transverse velocity, angular velocity, rate of twist, bending moment, shear, and twisting moment for the case of an infinite plate driven by a point moment are given, respectively, by:

$$\dot{\eta} = \frac{\omega M_p}{(8Bk)}\cos\phi\,[H_1^{(2)}(kr) + jH_1^{(2)}(-jkr)]e^{j\omega t}, \tag{A.65}$$

$$\dot{\theta}_b = \frac{\omega M_p}{(8B)}\cos\phi\, e^{j\omega t} \cdot \left[H_0^{(2)}(kr) + H_0^{(2)}(-jkr) - \frac{1}{(kr)}(H_1^{(2)}(kr) + jH_1^{(2)}(-jkr))\right], \tag{A.66}$$

$$\dot{\theta}_t = \frac{\omega M_p}{(8Bkr)}\sin\phi\,[H_1^{(2)}(kr) + jH_1^{(2)}(-jkr)]e^{j\omega t}, \tag{A.67}$$

$$M_b = \frac{jkM_p}{8}\cos\phi\left[\left[-H_1^{(2)}(kr) - \frac{1}{(kr)}H_0^{(2)}(kr) + \frac{2}{(kr)^2}H_1^{(2)}(kr)\right]\right.$$
$$j\left[-H_1^{(2)}(-jkr) + \frac{j}{(kr)}H_0^{(2)}(-jkr) - \frac{1}{(kr)^2}H_1^{(2)}(-jkr)\right] \tag{A.68}$$
$$\left. + \frac{\mu}{(kr)}[H_2^{(2)}(kr) + H_2^{(2)}(-jkr)]\right]e^{j\omega t},$$

$$Q = \frac{jk^2 M_p}{8}\cos\phi\, e^{j\omega t} \cdot \left[-H_0^{(2)}(kr) + \frac{1}{(kr)}H_1^{(2)}(kr) + H_0^{(2)}(-jkr) + \frac{j}{(kr)}H_1^{(2)}(-jkr)\right]. \tag{A.69}$$

$$M_t = \frac{jkM_p}{8}\sin\phi\frac{(1-\mu)}{(kr)}[H_2^{(2)}(kr) + H_2^{(2)}(-jkr)]e^{j\omega t}. \tag{A.70}$$

Solution for a Lateral Quadrupole

The solution for an infinite plate driven by a simple harmonic point lateral quadrapole can be obtained directly from the solution for a point moment by simple difierentiation with respect to the cartesian coordinate y. Thus, the solution for the transverse displacement due to a lateral quadrapole is given by

$$\eta = \frac{\partial}{\partial y}\frac{jQ_p}{(8Bk)}cos\phi\left[H_1^{(2)}(kr) + jH_1^{(2)}(-jkr)\right]e^{j\omega t}, \tag{A.71}$$

and from the calculus it is known that

$$\frac{\partial}{\partial y} = sin\phi\frac{\partial}{\partial r} + \frac{cos\phi}{r}\frac{\partial}{\partial\phi}.$$

Thus, the quadrapole solution is given by

$$\eta = \frac{jQ_p}{(8Bk)}e^{j\omega t}\bullet\left[cos\phi sin\phi\frac{\partial}{\partial r}\left[H_1^{(2)}(kr) + jH_1^{(2)}(-jkr)\right]\right.$$
$$\left. + \left[H_1^{(2)}(kr) + jH_1^{(2)}(-jkr)\right]\frac{cos\phi}{r}\frac{\partial}{\partial\phi}cos\phi\right]. \tag{A.72}$$

Carrying out the indicated operations and simplifying, the result is

$$\eta = \frac{jQ_p}{(8B)}cos\phi sin\phi\left[H_2^{(2)}(kr) + H_2^{(2)}(-jkr)\right]e^{j\omega t}. \tag{A.73}$$

38

Equations for transverse velocity, angular velocity, rate of twist, bending moment, shear, and twisting moment can be obtained, respectively, by straightforward differentiation of equation (A.73) using the formulae given by equations (A.59) through (A.64). Performing the operations indicated in these formulae on equation (A.73), the results are given by

$$\dot{\eta} = \frac{\omega Q_p}{(8B)} \cos\phi \sin\phi \left[H_2^{(2)}(kr) + H_2^{(2)}(-jkr) \right] e^{j\omega t}, \qquad (A.74)$$

$$\dot{\theta}_b = \frac{\omega Q_p}{(8B)} \cos\phi \sin\phi \, e^{j\omega t} \cdot \left[\left[H_1^{(2)}(kr) - j H_1^{(2)}(-jkr) \right] - \frac{2}{(kr)} \left[H_2^{(2)}(kr) + H_2^{(2)}(-jkr) \right] \right], \quad (A.75)$$

$$\dot{\theta}_t = \frac{\omega k Q_p \cos 2\phi}{(8B)} \frac{1}{(kr)} \left[H_2^{(2)}(kr) + H_2^{(2)}(-jkr) \right] e^{j\omega t}, \qquad (A.76)$$

$$M_b = \frac{jk^2 Q_p}{8} \cos\phi\sin\phi \, e^{j\omega t} \cdot \left[\left[-H_2^{(2)}(kr) + H_2^{(2)}(-jkr) \right] \right.$$
$$\frac{1}{(kr)} \left[H_1^{(2)}(kr) - j H_1^{(2)}(-jkr) \right] + \frac{6}{(kr)^2} \left[H_2^{(2)}(kr) + H_2^{(2)}(-jkr) \right]$$
$$\left. + \frac{\mu}{(kr)} \left[H_1^{(2)}(kr) - j H_1^{(2)}(-jkr) \right] - \frac{\mu 6}{(kr)^2} \left[H_2^{(2)}(kr) + H_2^{(2)}(-jkr) \right] \right], \qquad (A.77)$$

$$Q = \frac{jk^3 Q_p}{8} \cos\phi\sin\phi \, e^{j\omega t} \cdot \left[\left[H_1^{(2)}(kr) + j H_1^{(2)}(-jkr) \right] \right.$$
$$\left. + \frac{2}{(kr)} \left[H_2^{(2)}(kr) + H_2^{(2)}(-jkr) \right] \right], \qquad (A.78)$$

$$M_t = (1 - \mu) \frac{jk^2 Q_p}{8} \cos 2\phi \, e^{j\omega t} \cdot \left[\frac{1}{(kr)} \left[H_1^{(2)}(kr) - j H_1^{(2)}(-jkr) \right] \right.$$
$$\left. - \frac{3}{(kr)^2} \left[H_2^{(2)}(kr) - H_2^{(2)}(-jkr) \right] \right]. \qquad (A.79)$$

39

APPENDIX III

EQUATIONS FOR THE TRANSVERSE VIBRATION
OF BEAMS NEAR TO SIMPLE BOUNDARIES

Introduction

This appendix is largely a recapitulation of the theory developed by B. R. Mace in reference 8. For more detailed explanations of the concepts presented here see reference 8.

As shown in Appendix I, the solution for the transverse displacement in a beam due to a simple harmonic disturbance is given by equation (A.7) (repeated here for the convenience of the reader)

$$\eta(x,t) = [C_1 e^{-jkx} + C_2 e^{jkx} + C_3 e^{-kx} + C_4 e^{kx}] e^{j\omega t}, \qquad (A.7)$$

where the wavenumber k is given by $k^4 = m\omega^2/B$. It should be noted that the coefficients in equation (A.7) may have complex values. Also note that C_1 and C_3 correspond to the propagating and decaying portions of a right traveling wave, respectively. Similarly, C_2 and C_4 correspond to the propagating and decaying portions of a left traveling wave, respectively.

Now define the following vectors

$$a^+ = \begin{pmatrix} C_1 \\ C_3 \end{pmatrix}, \qquad a^- = \begin{pmatrix} C_2 \\ C_4 \end{pmatrix} \qquad (A.80)$$

and also define the following matrices

$$[f] = \begin{pmatrix} e^{-jkx} & 0 \\ 0 & e^{-kx} \end{pmatrix} \quad ; \quad [f]^{-1} = \begin{pmatrix} e^{+jkx} & 0 \\ 0 & e^{+kx} \end{pmatrix}. \tag{A.81}$$

Utilizing equations (A.80) and (A.81), a vector describing the magnitude of the transverse displacement of the beam at any location x can be expressed as

$$\vec{a}(x) = ([f]\vec{a}^+ + [f]^{-1}\vec{a}^-), \tag{A.82}$$

and at the position $x = 0$ this vector is given by

$$\eta(0, t) = ([I]\vec{a}^+ + [I]\vec{a}^-), \tag{A.83}$$

where $[I]$ is the identity matrix.

Utilizing equation (A.82), define the following vectors:

$$\vec{a}^+(x) = [f]\vec{a}^+; \qquad \vec{a}^-(x) = [f]^{-1}\vec{a}^-. \tag{A.84}$$

Using equation (A.84) it can be shown that the amplitudes of the displacement, slope, bending moment, and shear of the beam at any location x can be computed using the following matrix equation (see reference 8):

41

$$
\begin{pmatrix}
\eta \\
(1/k)d\eta/dx \\
M/(EIk^2) \\
Q/(EIk^3)
\end{pmatrix}
\quad
\begin{pmatrix}
1 & 1 \\
-j & -1 \\
1 & 1 \\
j & 1
\end{pmatrix}
a^+(x) +
\begin{pmatrix}
1 & 1 \\
j & 1 \\
1 & 1 \\
j & 1
\end{pmatrix}
a^-(x).
\qquad (A.85)
$$

Wave Reflection at Point Discontinuities

Now assume that the location $x = 0$ coincides with the location of a point discontinuity (boundary) which is characterized by the following dimensionless translational and rotational stiffness parameters, respectively:

$$
K_\eta \quad (-\omega^2 m_\eta + j\omega 2\xi_\eta(k_\eta m_\eta)^{1/2} + k_\eta)/(EIk^3), \qquad (A.86)
$$

$$
K_\theta \quad (-\omega^2 m_\theta + j\omega 2\xi_\theta(k_\theta m_\theta)^{1/2} + k_\theta)/(EIk), \qquad (A.87)
$$

Further suppose that a set of right traveling waves represented by a^+ is incident on this boundary and gives rise to a set of reflected (left traveling) waves represented by a^- given by the equation

$$
a^- = r\, a^+, \qquad (A.88)
$$

where r is the reflection matrix.

42

It is shown in reference 8 that the reflection matrix $[r]$, for a boundary characterized by equations (A.86) and (A.87), is given by the equation

$$[r] = C_\eta \begin{pmatrix} j & j \\ 1 & 1 \end{pmatrix} + C_\theta \begin{pmatrix} -j & -1 \\ j & 1 \end{pmatrix}, \qquad (A.89)$$

where

$$C_\eta = \frac{K_\eta}{[4 - (1 + j)\overline{K_\eta}]}, \qquad (A.90)$$

and

$$C_\theta = \frac{K_\theta}{[4 + (1 - j)\overline{K_\theta}]}. \qquad (A.91)$$

Substituting equation (A.89) into equation (A.84), the vectors for the right traveling and left traveling components of the transverse displacement at any location on the incident side of the beam ($r = 0$) are given by

$$a^+(r) = [f]a^+; a^-(r) = [f]^{-1}[r]a^+. \qquad (A.92)$$

The vector equations given by (A.92) can now be substituted into the vector equation of (A.85). Thus, equation (A.85) can be used to calculate the transverse

43

displacement, the slope, the bending moment, and the shear of the beam at any location on the incident side of the beam ($r = 0$). The transverse and angular velocities of the beam can then be obtained from the transverse displacement and slope of the beam, respectively, by differentiation with respect to time.

REFERENCES

1. Noiseux, D.U.: "Measurement of Power flow in Uniform Beams and Plates," Journal of the Acoustic Society of America, Vol. 47, No. 1, 1970.

2. Pavic, G.: "Techniques for the Determination of Vibration Transmission Mechanisms in Structures," Ph.D. dissertation, University of Southhampton, England, 1976.

3. Carroll, G.P. and Clark, J.A.: "Four Accelerometer Structural Vibration Intensity Measurements on Beams," Presented at the 106th meeting of the Acoustical Society of America, 1983.

4. Quinlin, D.A.: "Measurement of Complex Intensity and Potential Energy Density in Structural Bending Waves," Master's thesis in Acoustics, Pennsylvania State University, 1985.

5. Redman-White, W.: "The Measurement of Structural Wave Intensity," Ph.D. Dissertation, University of Southampton, England, 1983.

6. Cremer, L.; Heckl, M.; Ungar, E.E.: "Structure-Borne Sound," Springer-Verlag, Berlin-Heidelberg, 1973.

7. Mickol, J.: "An Investigation of Energy Transmission Due to Flexural Wave Propagation in Lightweight Built-Up Structures," Master's Thesis, Purdue University, 1986.

8.   Mace, B.R.: "Wave Reflection and Transmission in Beams," Journal of Sound and Vibration, Vol. 97, No. 2, 1984.

46

TABLE I. - MATERIAL PROPERTIES OF THE PLATE

Material	Young's modulus N/m^2	Poisson's ratio	Thickness cm	Density kg/m^3
AA2024	$0.7309 *10^{11}$	0.330	0.3175	$0.2794 *10^4$
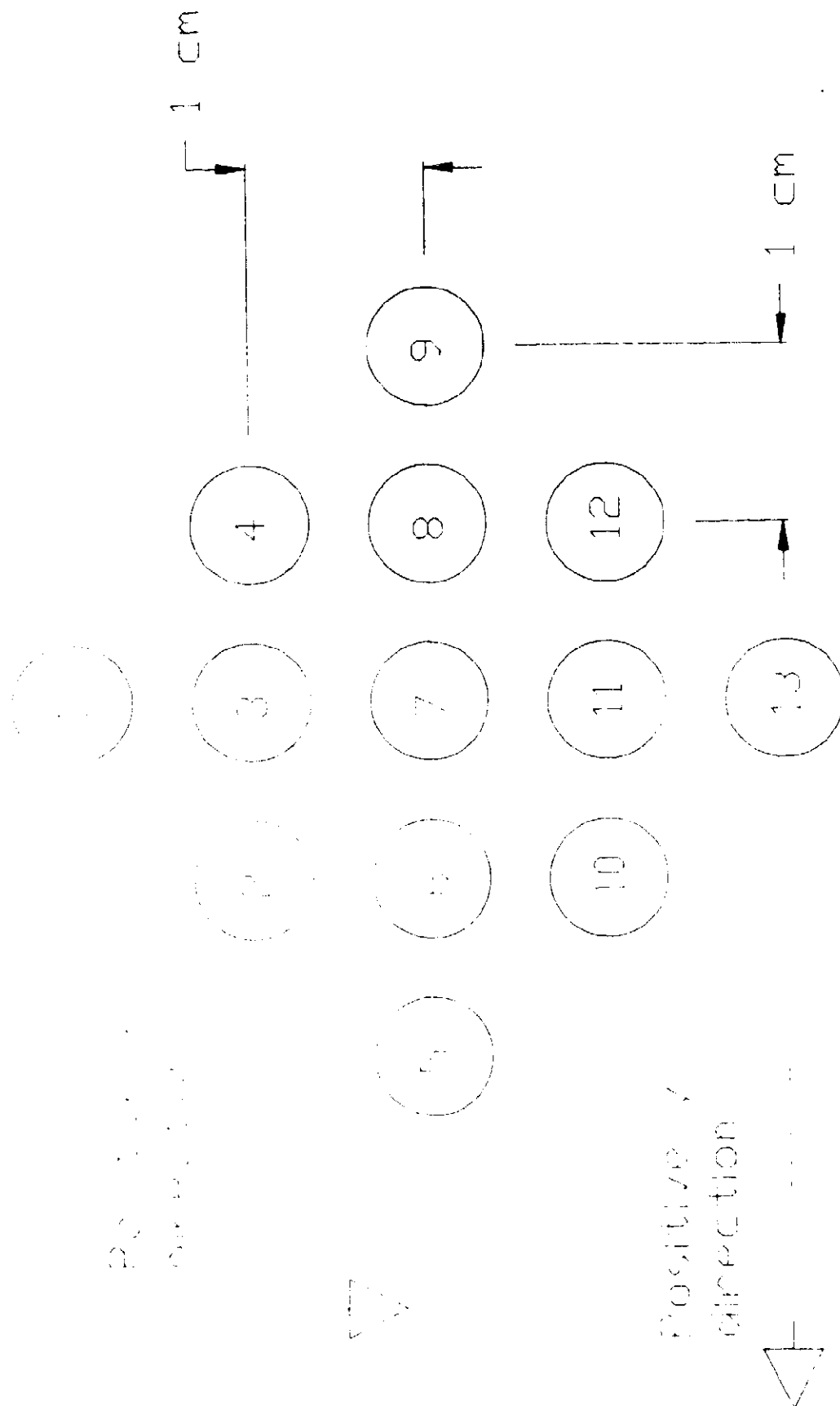
Figure 1 – Computational molecule for the direct finite difference approach.
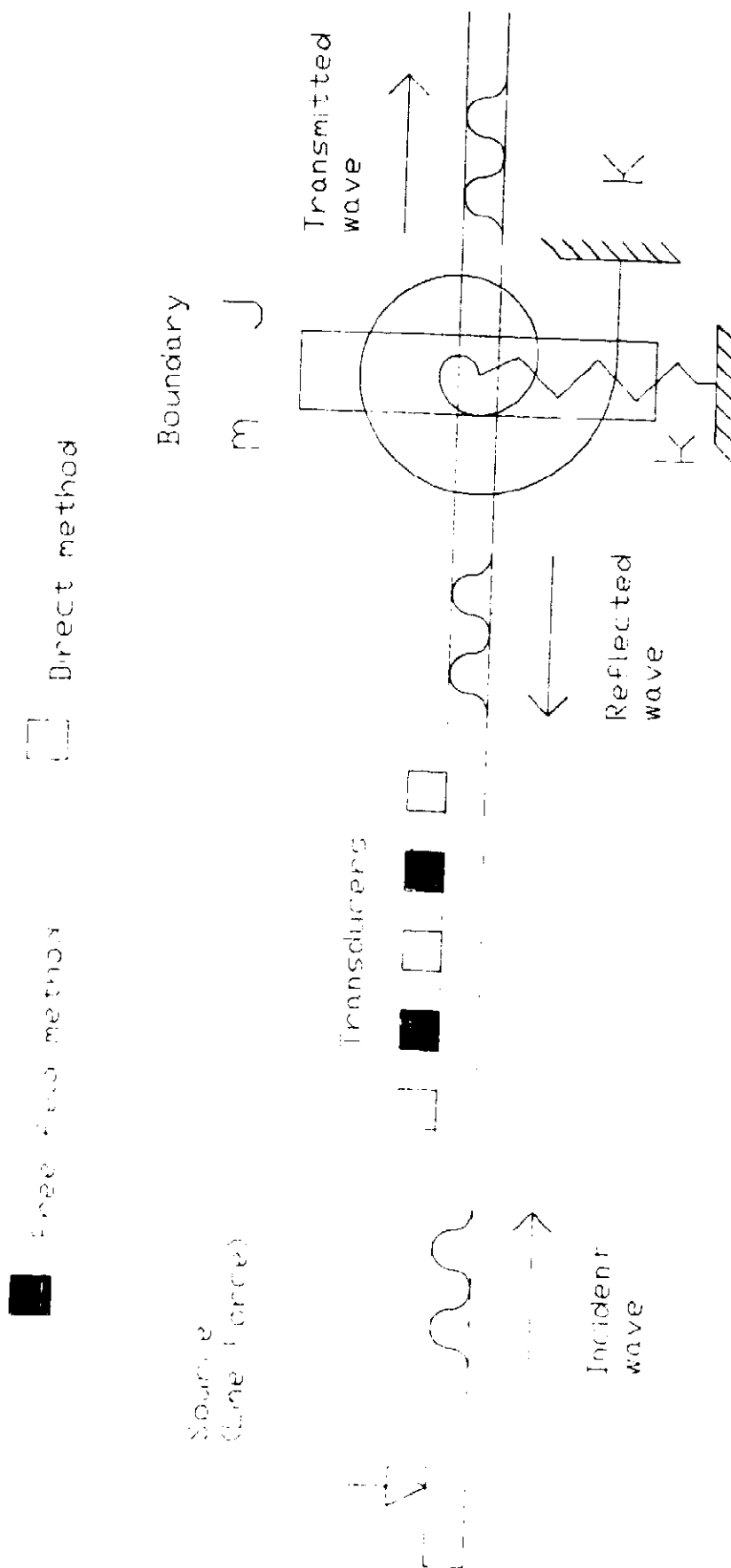
Figure 2 – Geometry for the simulation of measurements near to simple boundaries.
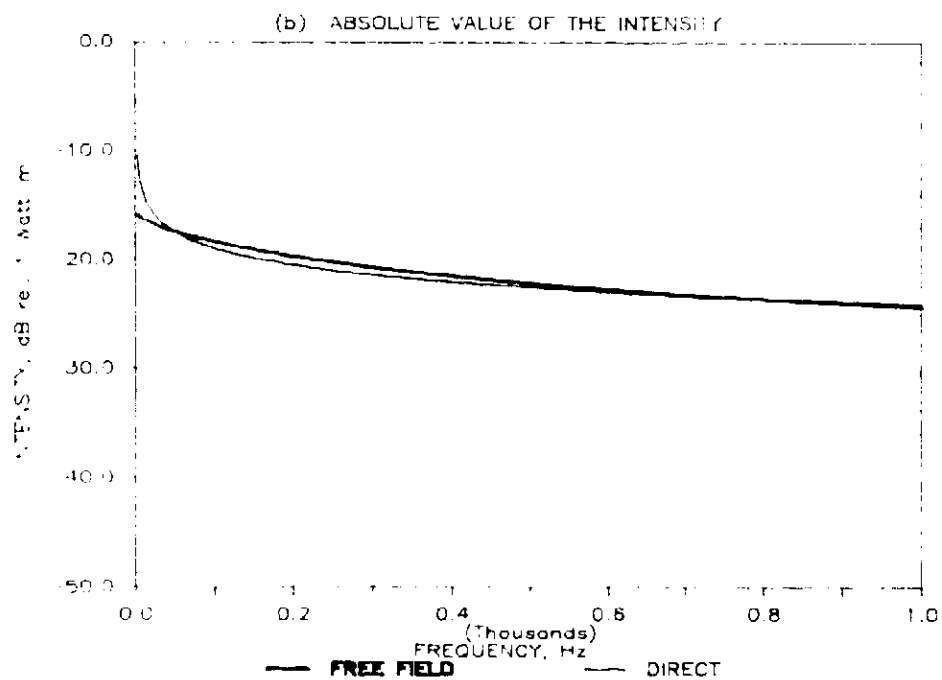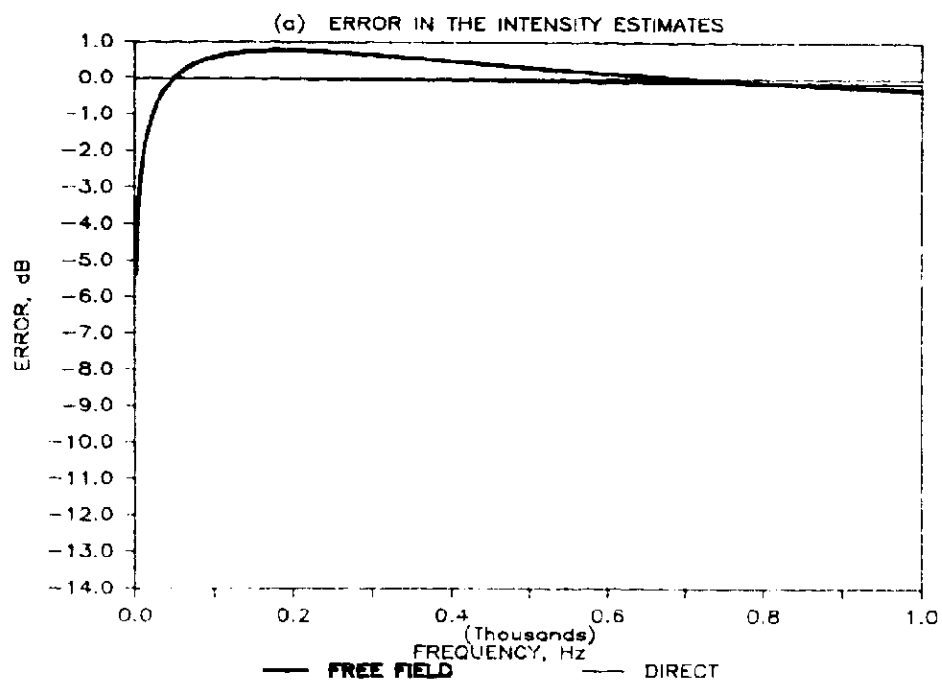
Figure 3 - Simulated measurements 10 cm from a line force.
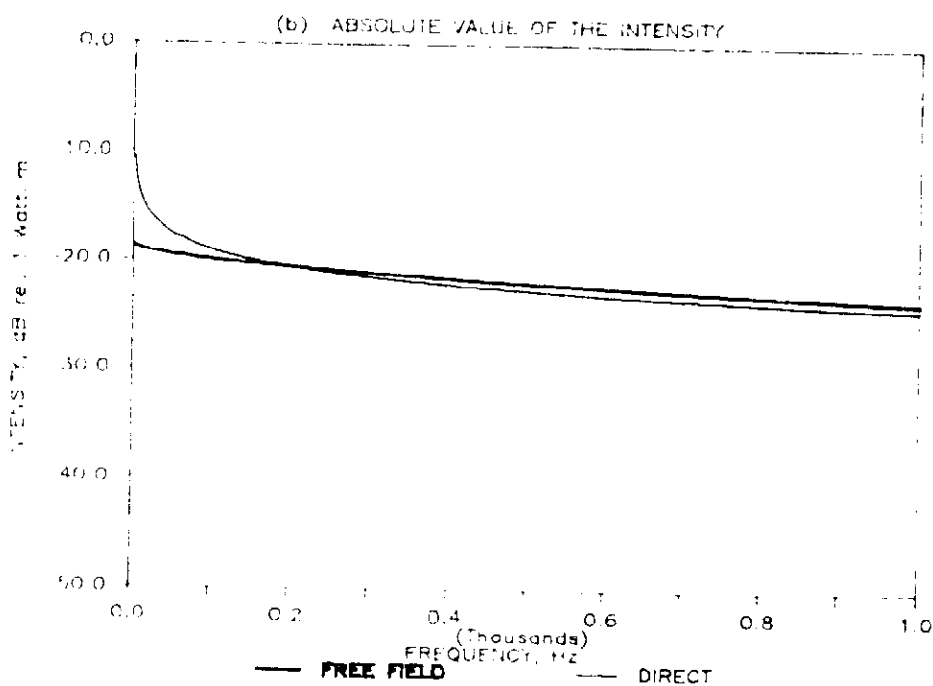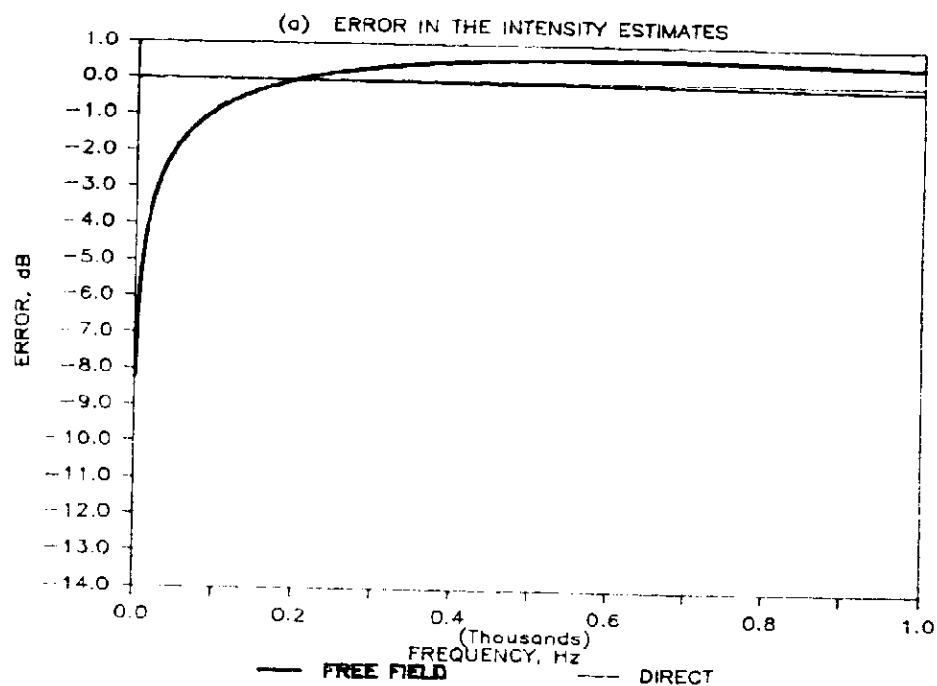
Figure 4 – Simulated measurements 5 cm from a line force.
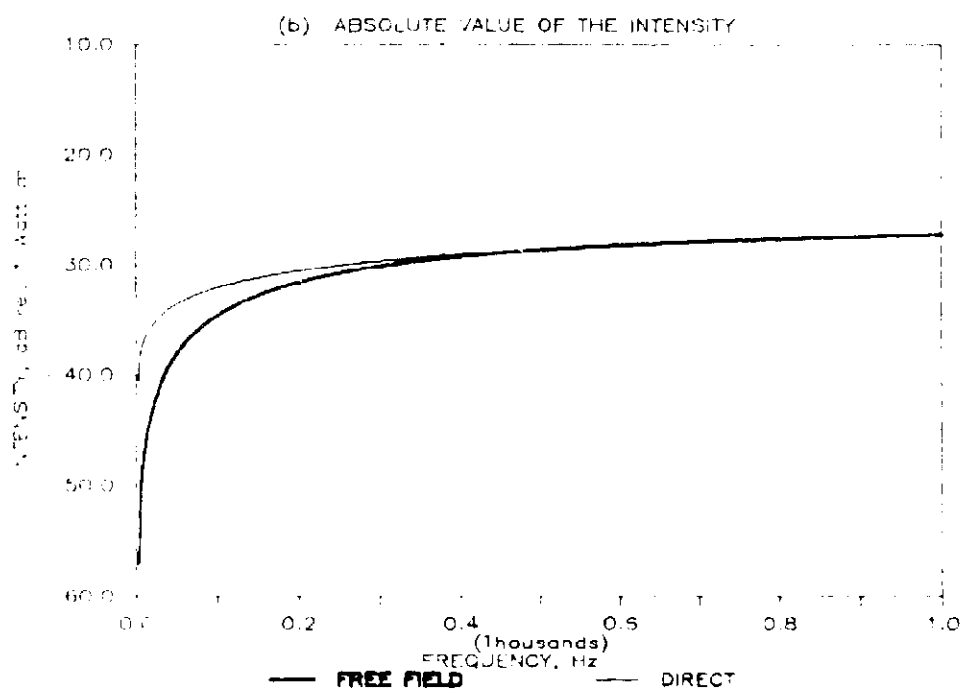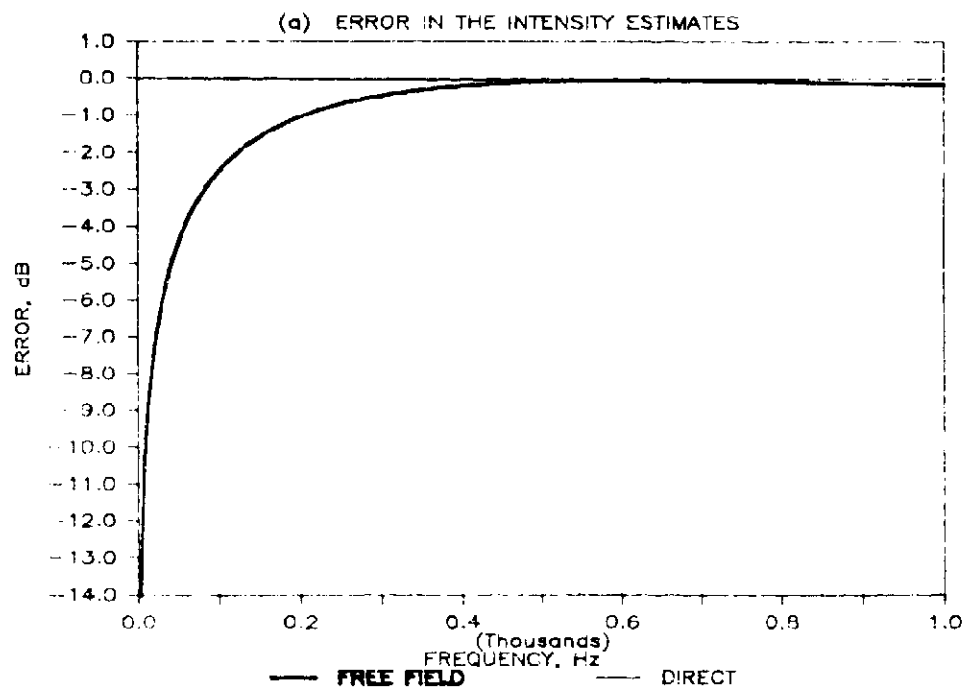
Figure 5 - Simulated measurements 10 cm from a line moment.
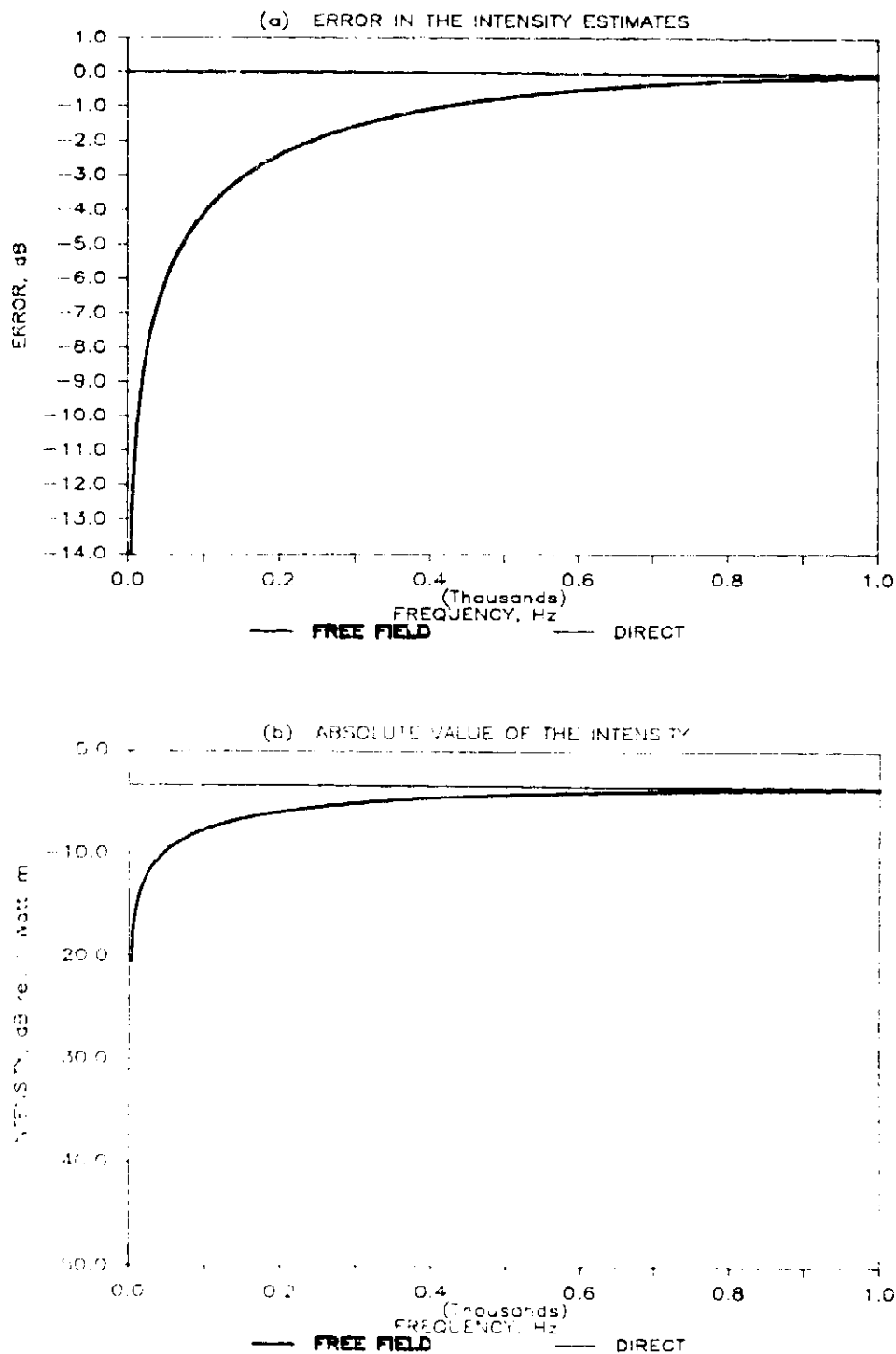
Figure 6 – Simulated measurements 5 cm from a point force.
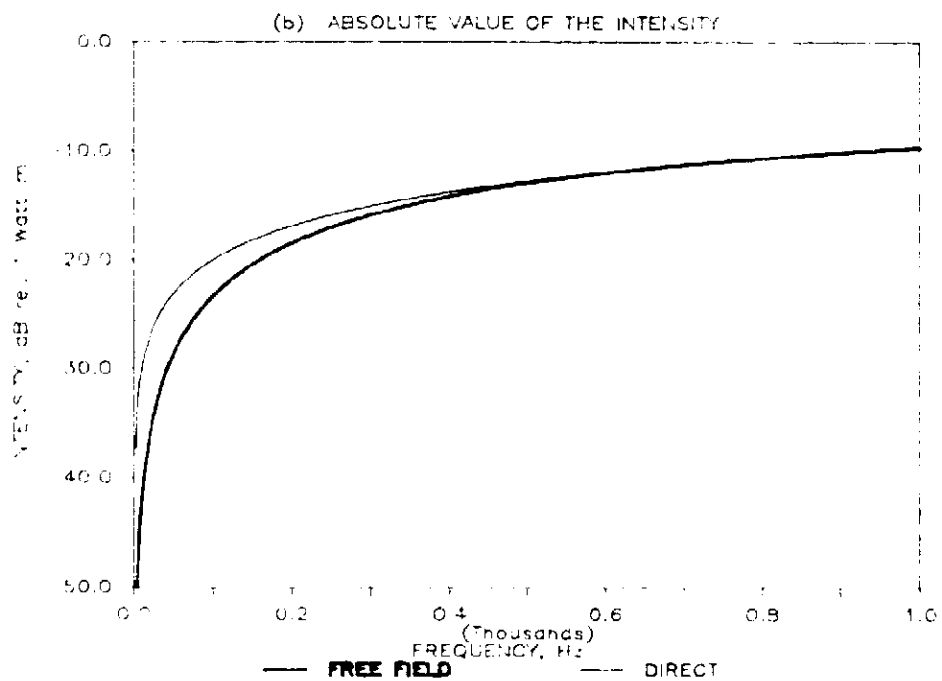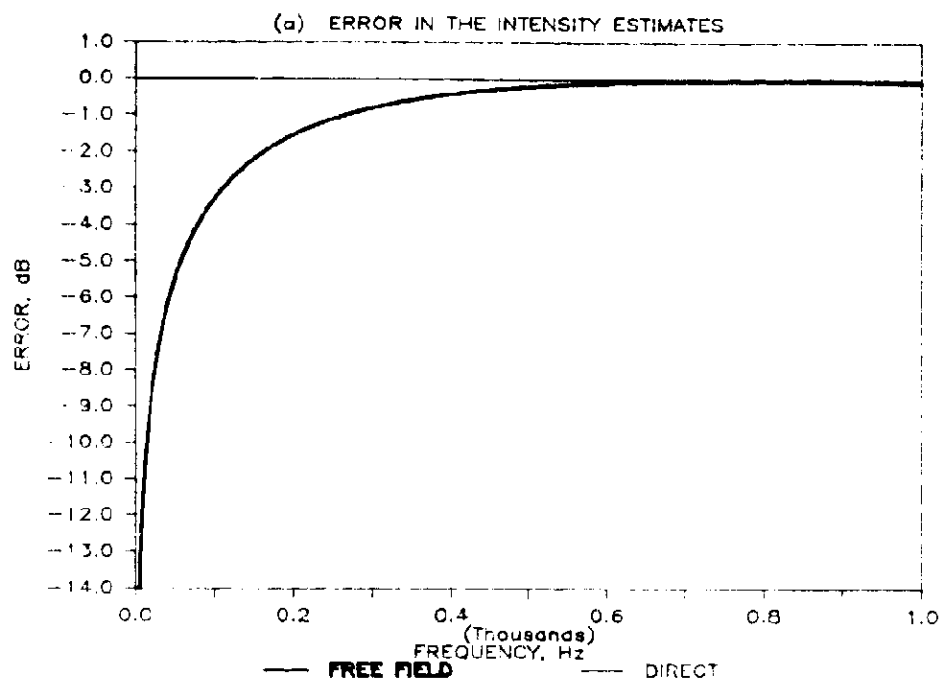
Figure 7 - Simulated measurements 10 cm from a point moment
at an azimuthal angle of 0 degrees.
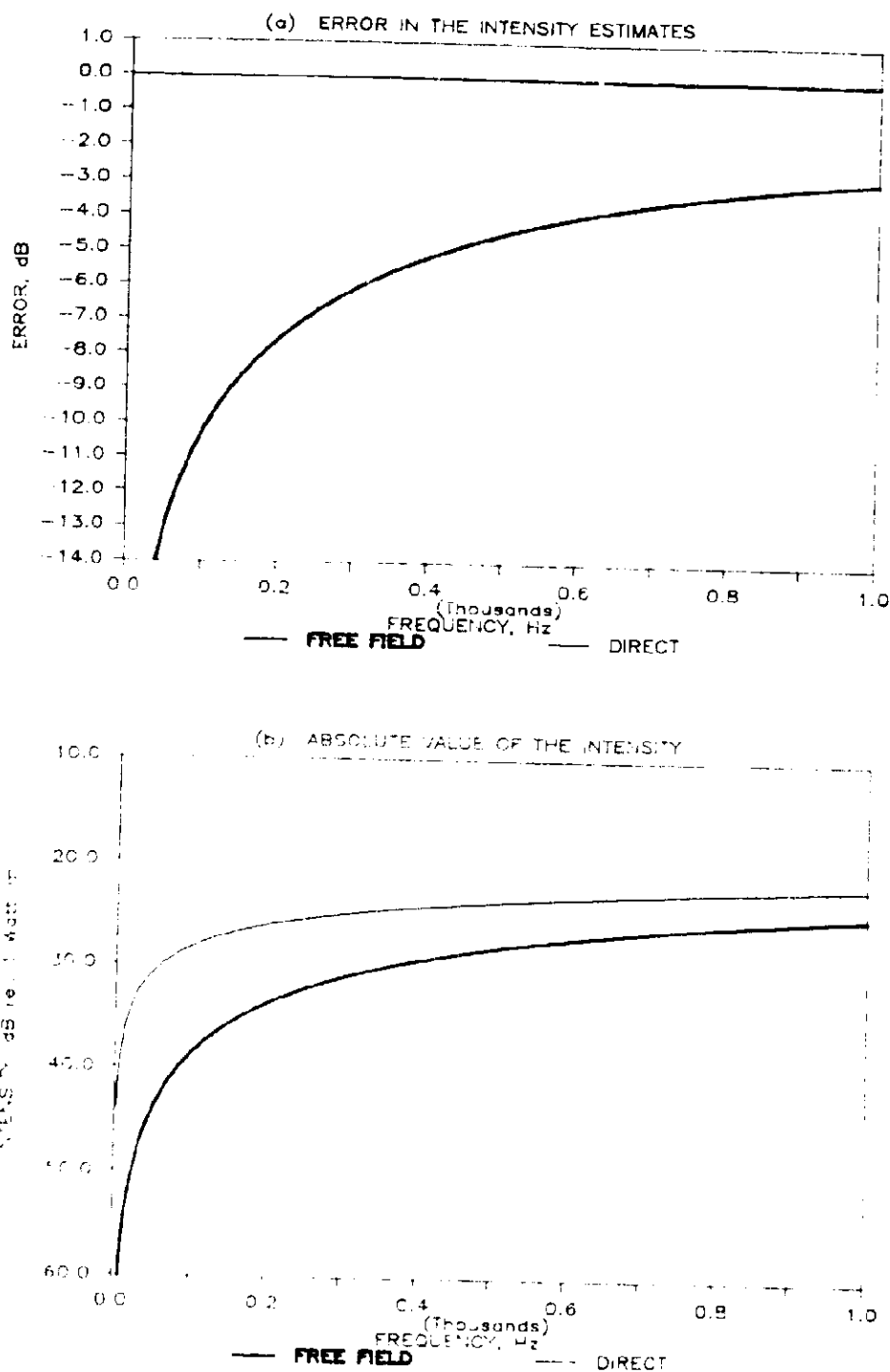
Figure 8 - Simulated measurements 10 cm from a point moment at an azimuthal angle of 80 degrees.

(a) ERROR IN THE INTENSITY ESTIMATES

(b) ABSOLUTE VALUE OF THE INTENSITY
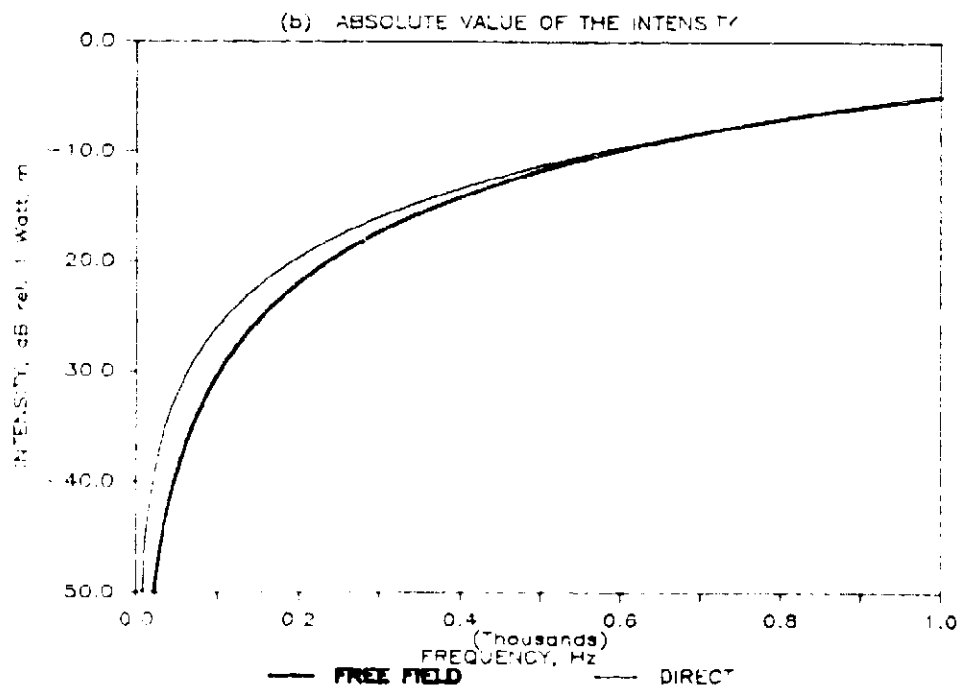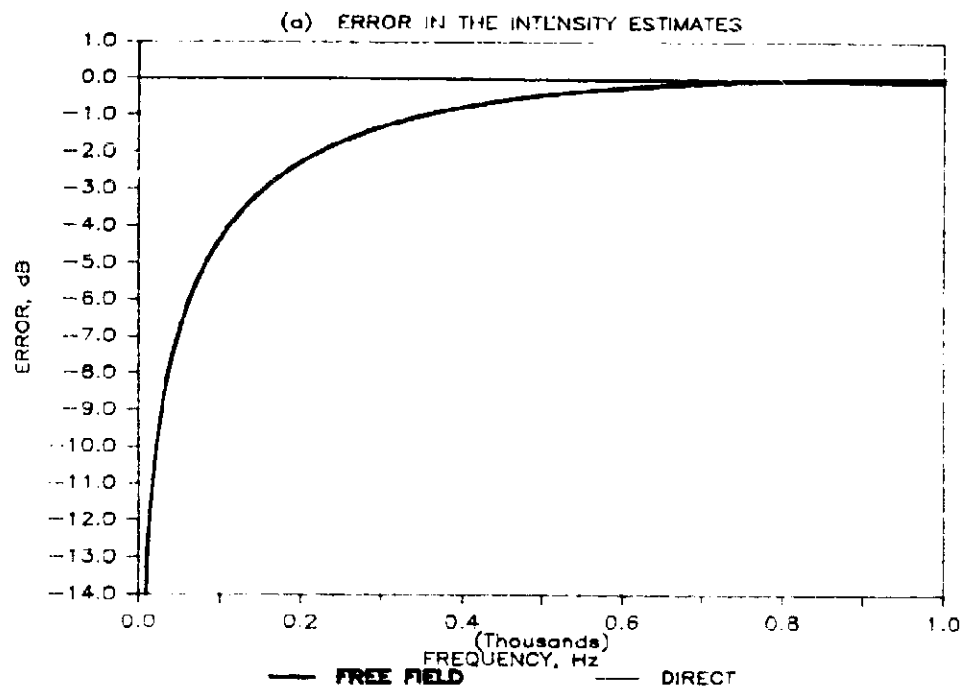
Figure 9 - Simulated measurements 10 cm from a
quadrupole at an azimuthal angle of 45 degrees.
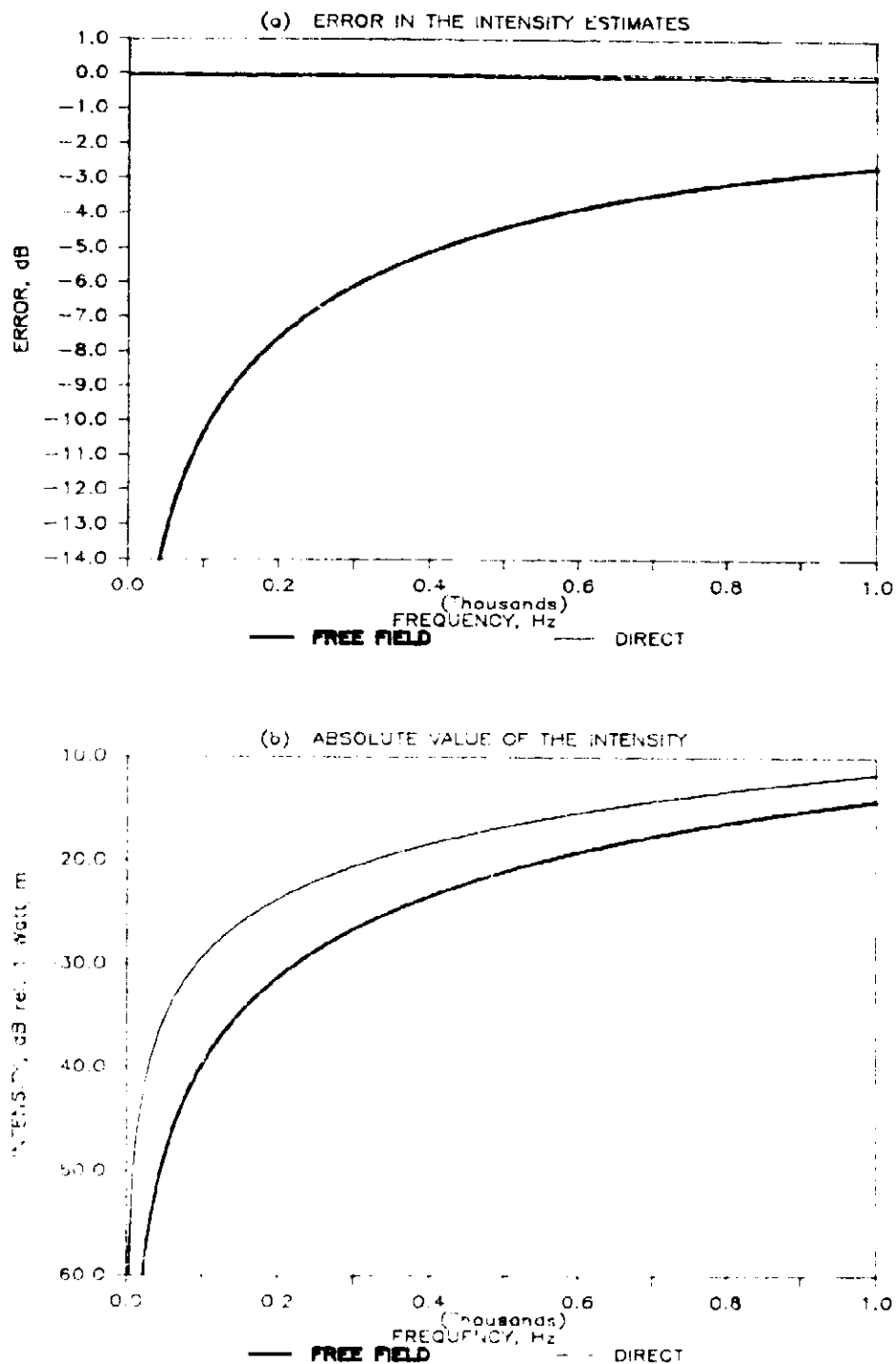
Figure 10 - Simulated measurements 10 cm from a
quadrupole at an azimuthal angle of 10 degrees.

(a) ERROR IN THE INTENSITY ESTIMATES

(b) ABSOLUTE VALUE OF THE INTENSITY
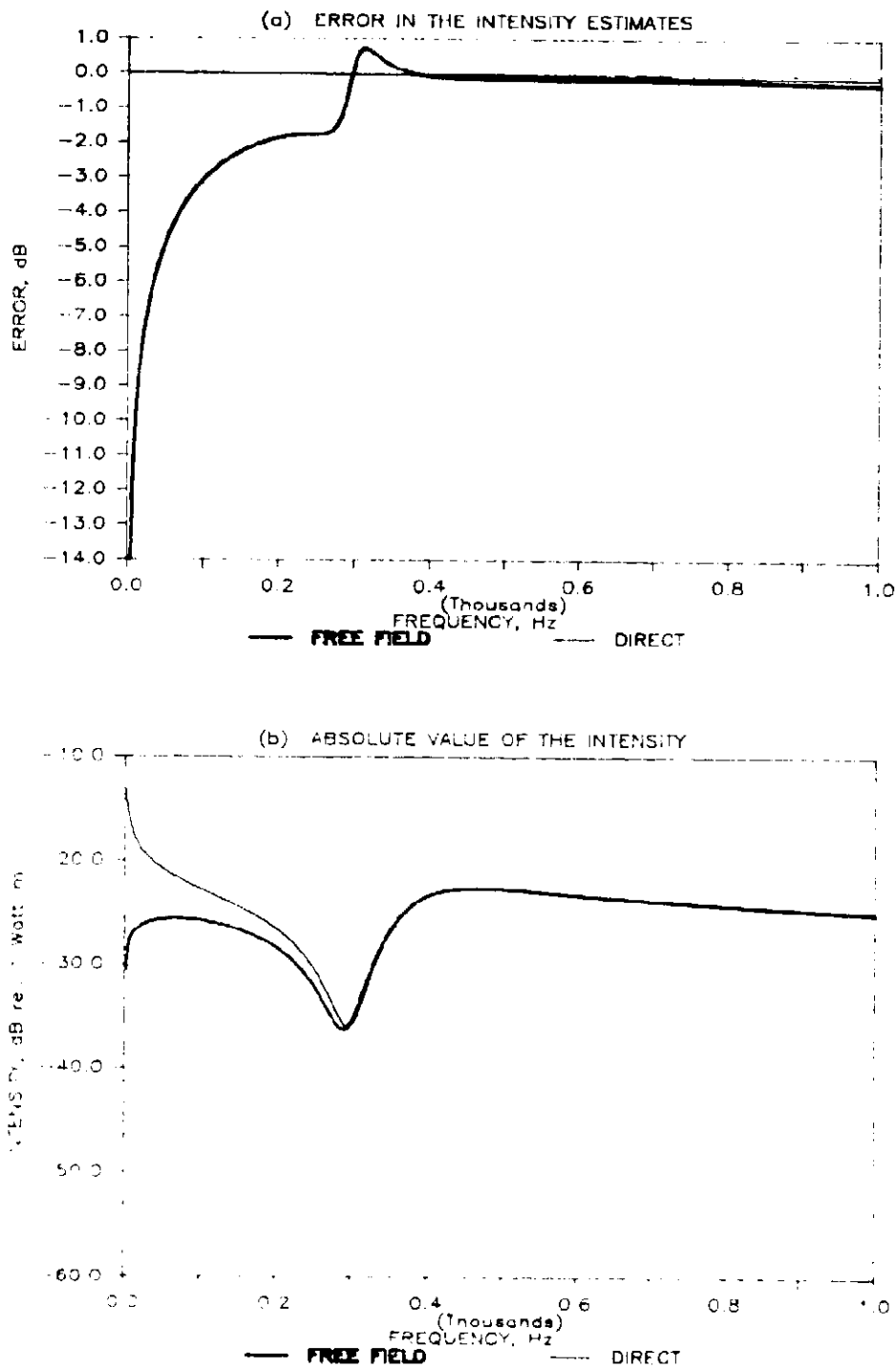
Figure 11 - Simulated measurements 10 cm from a line boundary which possesses translational stiffness and inertia.

(a) ERROR IN THE INTENSITY ESTIMATES

(b) ABSOLUTE VALUE OF THE INTENSITY
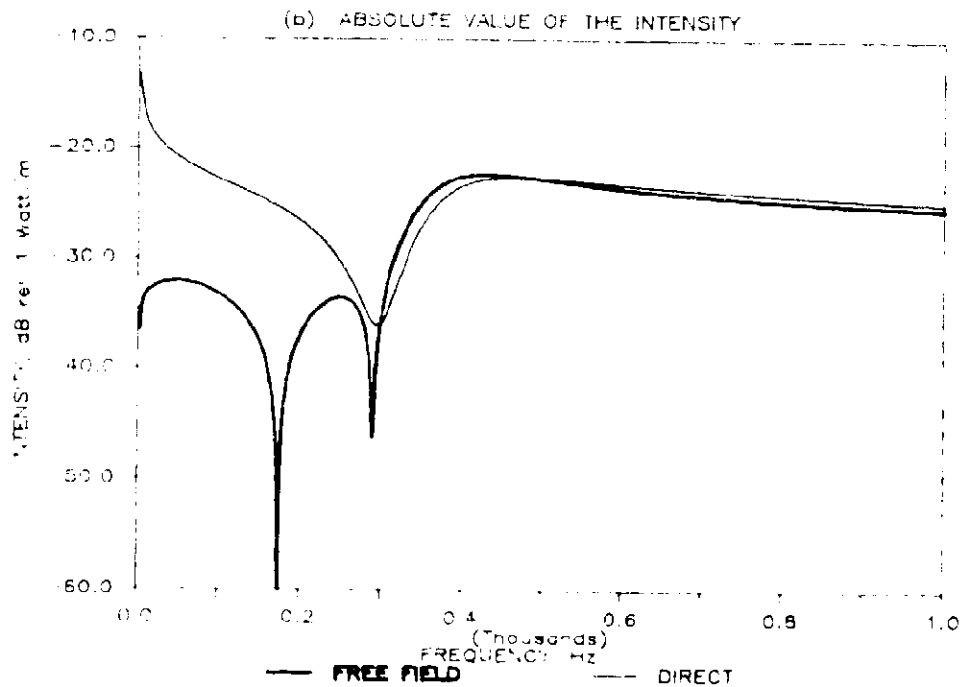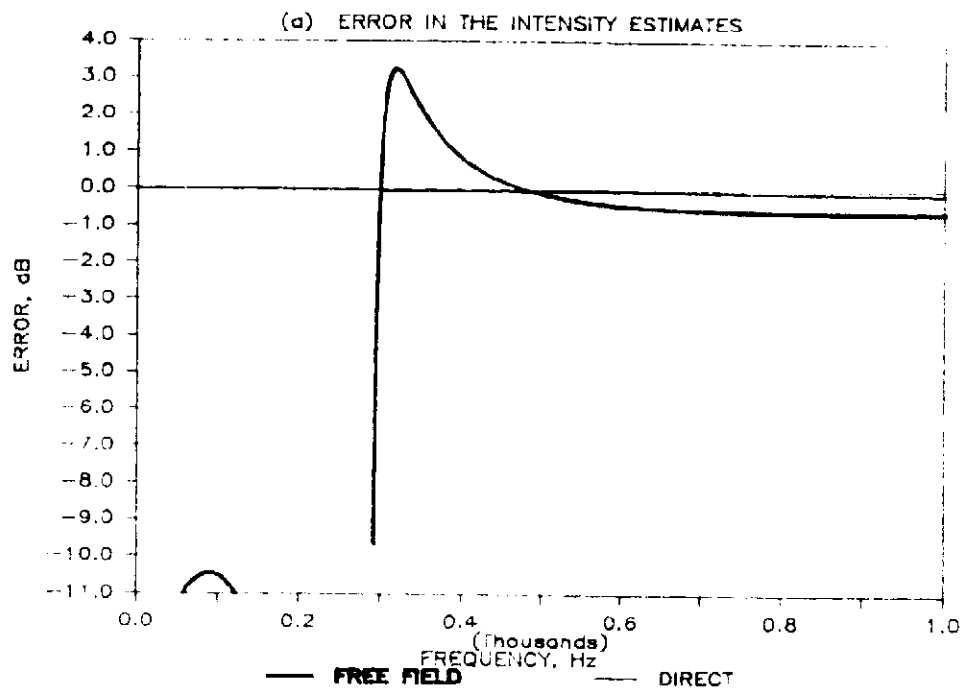
Figure 12 - Simulated measurements 5 cm from a line boundary which possesses translational stiffness and inertia.
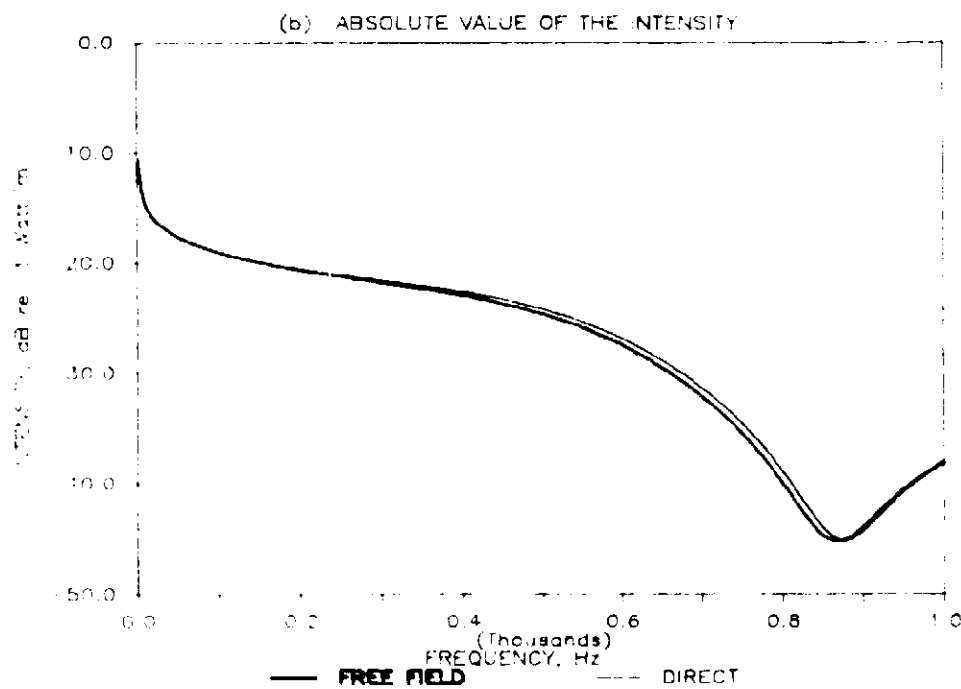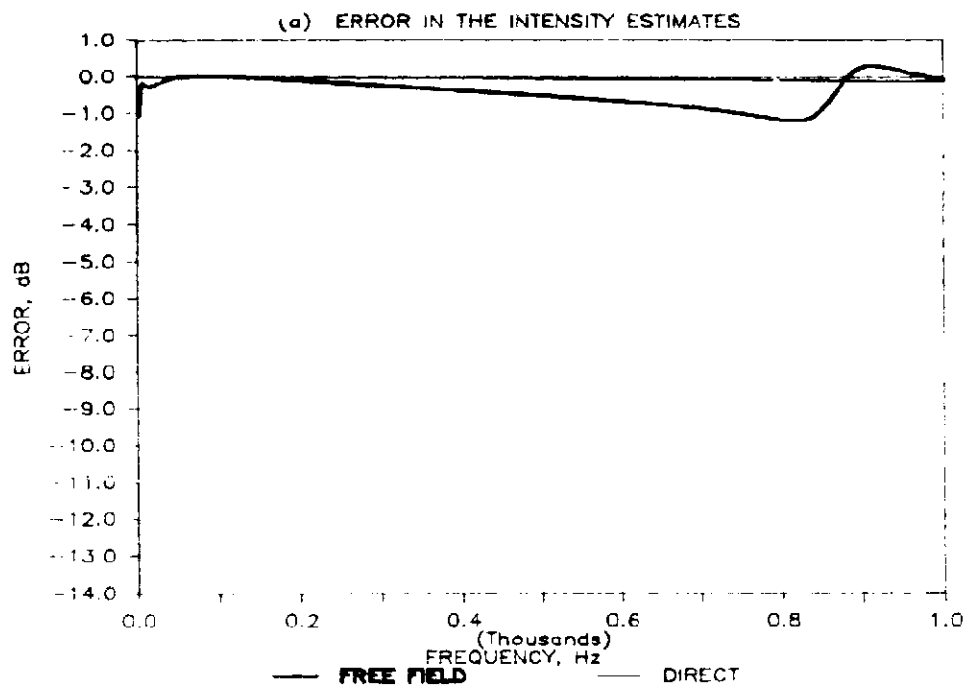
Figure 13 – Simulated measurements 10 cm from a line boundary which possesses rotational stiffness and inertia.
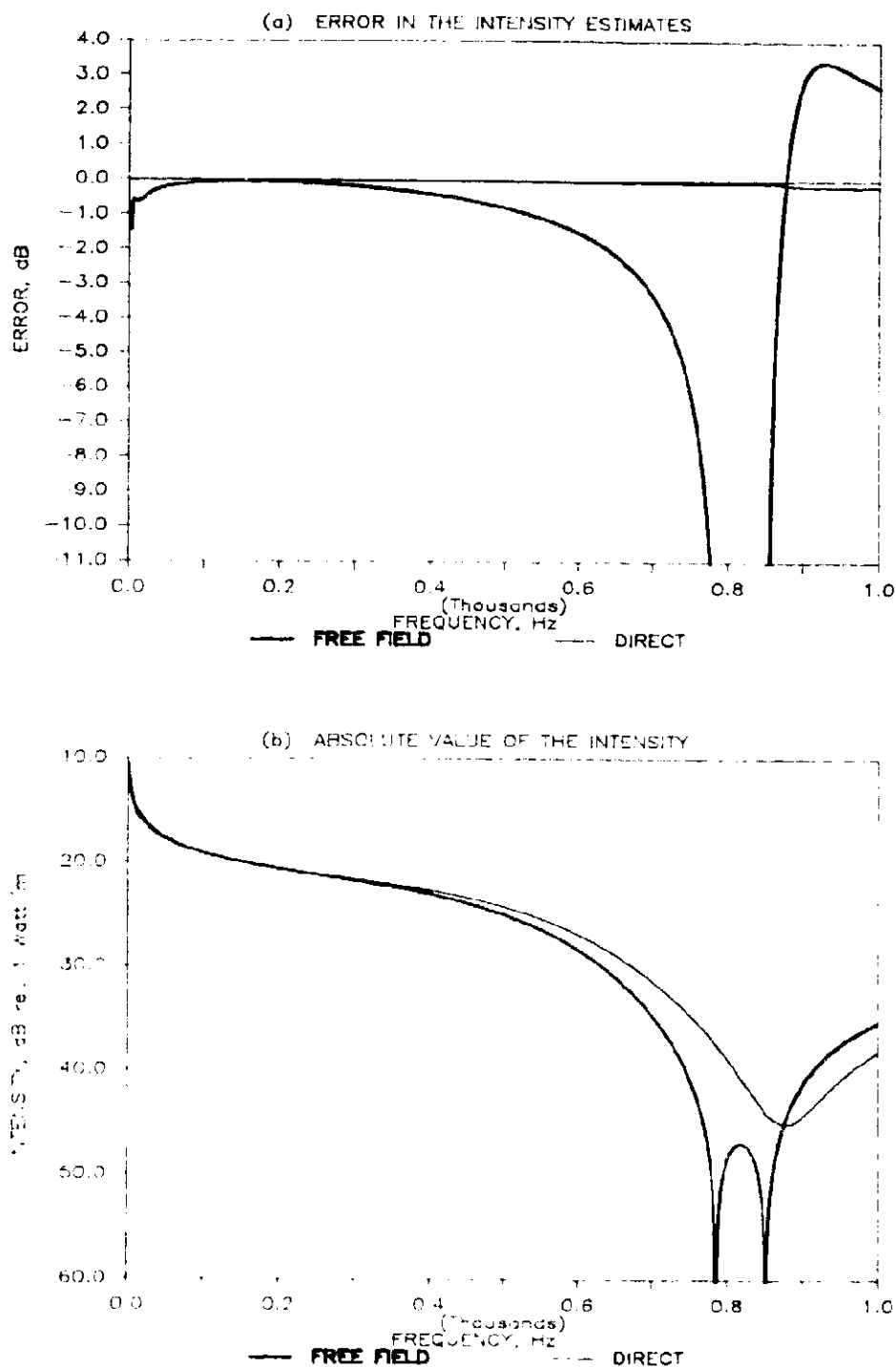
Figure 14 - Simulated measurements 5 cm from a line boundary which possesses rotational stiffness and inertia.

(a) ERROR IN THE INTENSITY ESTIMATES

(b) ABSOLUTE VALUE OF THE INTENSITY

Figure 15 - Simulated measurements 10 cm from a line boundary which possesses both rotational and translational properties.

(a) ERROR IN THE INTENSITY ESTIMATES

(b) ABSOLUTE VALUE OF THE INTENSITY
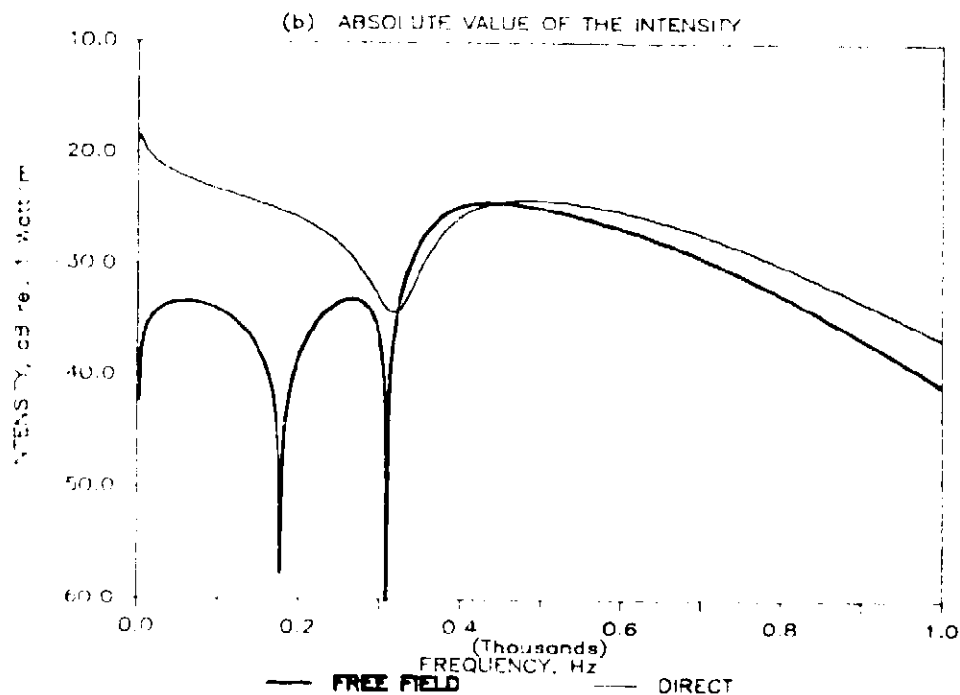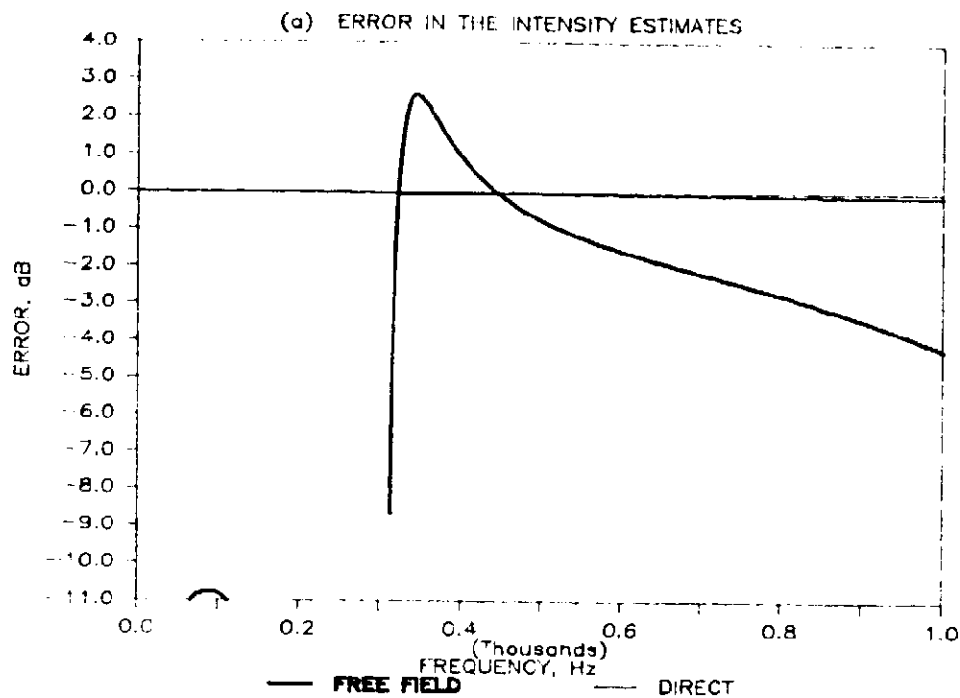
Figure 16 - Simulated measurements 5 cm from a line boundary
which possesses both rotational and translational
properties.

(a) ERROR IN THE INTENSITY ESTIMATES

(b) ABSOLUTE VALUE OF THE INTENSITY
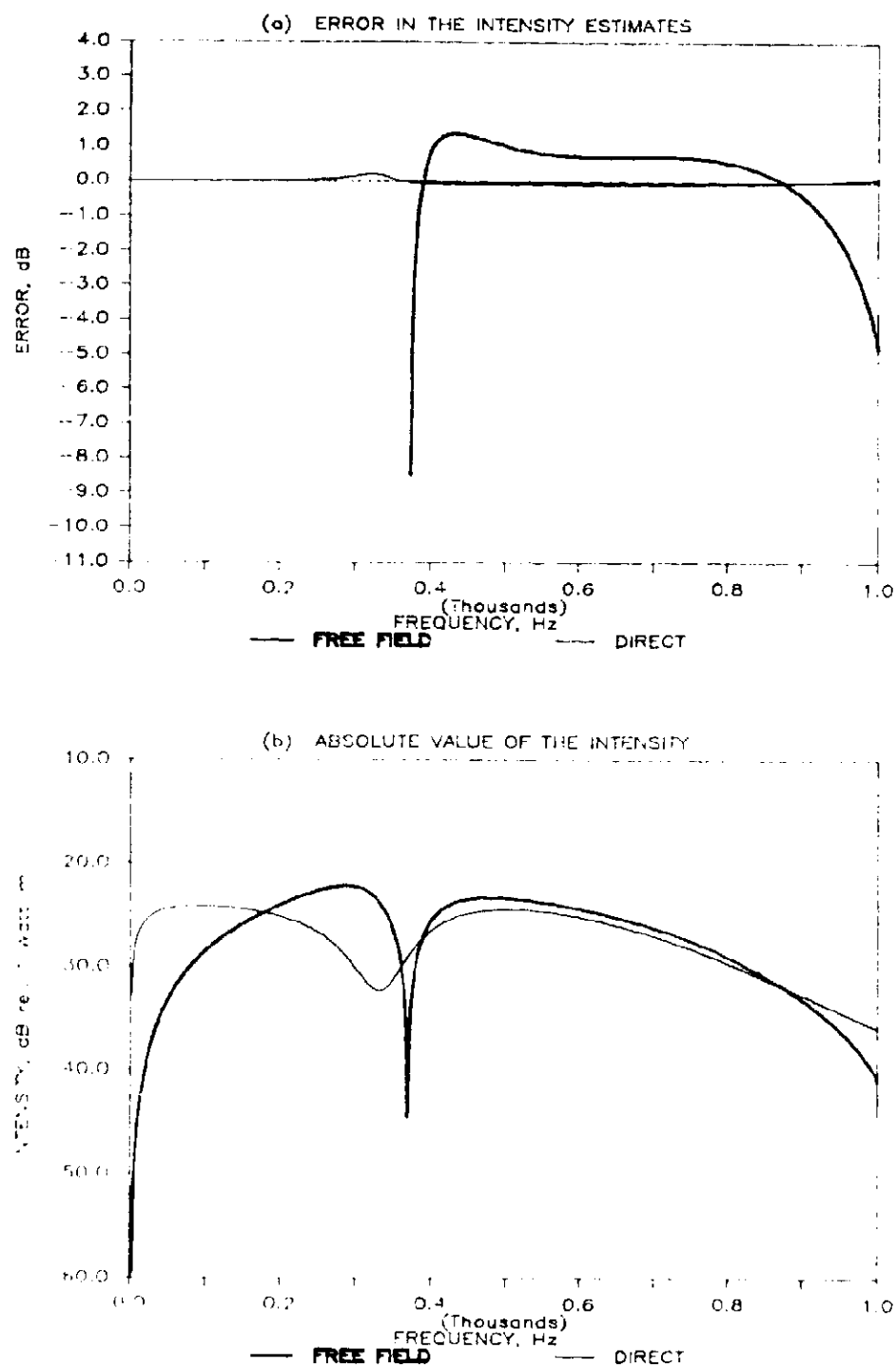
Figure 17 – Simulated measurements in the combined near fields of a source and a boundary.

16. Abstract

Recent advances in electronics technology along with the advent of low cost multi-channel Fast Fourier analyzers have now made it practical to use higher order central difference formulae to measure power flow in one dimensional and two dimensional structures. The method discussed in this paper uses five point differencing for the spatial derivatives in one dimensional and a thirteen point difference pattern for the spatial derivatives in two dimensional plates and shells. It is assumed that the measuring transducers are accelerometers.

An analytical study of the higher order differencing method and the conventional two accelerometer method was performed here as a preliminary to the application of these methods to actual aircraft structures. Some classical problems were analyzed in order to simulate and compare the performance of the two methods under near field measurement conditions. Near field conditions analyzed in this study include examples of power flows near simple sources and simple boundaries. The estimates produced by the two methods were compared to the exact solution in each example. This paper presents the theory and selected results of the study. The results indicate that the bias errors of the two accelerometer method under near field measurement conditions may be much larger than previous studies have suggested.